Article

Developmental Cell

Local Auxin Biosynthesis Is a Key Regulator of Plant Development

Graphical Abstract

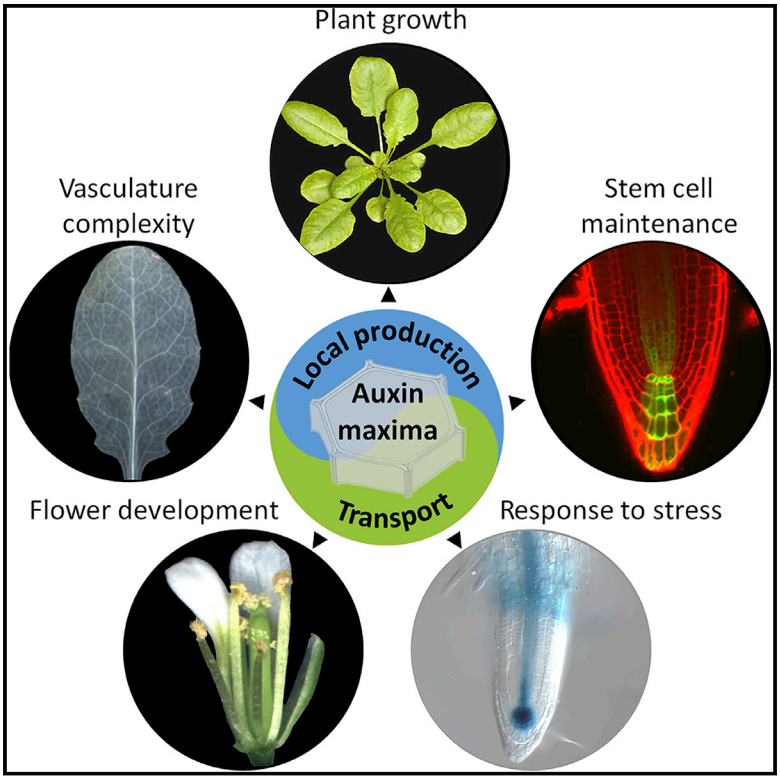

Authors

Javier Brumos, Linda M. Robles, Jeonga Yun, Thien C. Vu, Savannah Jackson, Jose M. Alonso, Anna N. Stepanova

Correspondence

atstepan@ncsu.edu

In Brief

The plant hormone auxin is a key regulator of plant growth and development. Brumos et al. show that local biosynthesis and polar transport of auxin act in concert to produce robust auxin maxima in the root quiescent center to sustain the meristematic potential of the root stem cell niche.

Highlights

- Local auxin production in roots is required for maintaining functional root meristems
- Local biosynthesis and transport of auxin cooperate at generating robust auxin maxima
- Auxin produced in the root quiescent center is sufficient for root meristem viability

Brumos et al., 2018, Developmental Cell *47*, 306–318
November 5, 2018
https://doi.org/10.1016/j.devcel.2018.09.022

CellPress

CellPress

Developmental Cell
Article

Local Auxin Biosynthesis Is a Key Regulator of Plant Development

Javier Brumos,[1] Linda M. Robles,[1] Jeonga Yun,[1] Thien C. Vu,[1] Savannah Jackson,[1] Jose M. Alonso,[1] and Anna N. Stepanova[1,2,*]

[1]Department of Plant and Microbial Biology, Program in Genetics, North Carolina State University, Raleigh, NC 27695-7614, USA
[2]Lead Contact
*Correspondence: atstepan@ncsu.edu
https://doi.org/10.1016/j.devcel.2018.09.022

SUMMARY

Auxin is a major phytohormone that controls numerous aspects of plant development and coordinates plant responses to the environment. Morphogenic gradients of auxin govern cell fate decisions and underlie plant phenotypic plasticity. Polar auxin transport plays a central role in auxin maxima generation. The discovery of the exquisite spatiotemporal expression patterns of auxin biosynthesis genes of the *WEI8/TAR* and *YUC* families suggested that local auxin production may contribute to the formation of auxin maxima. Herein, we systematically addressed the role of local auxin biosynthesis in plant development and responses to the stress phytohormone ethylene by manipulating spatiotemporal patterns of *WEI8*. Our study revealed that local auxin biosynthesis and transport act synergistically and are individually dispensable for root meristem maintenance. In contrast, flower fertility and root responses to ethylene require local auxin production that cannot be fully compensated for by transport in the generation of morphogenic auxin maxima.

INTRODUCTION

Nearly every aspect of a plant's life is influenced by auxin. Not only does this phytohormone govern many developmental programs of the plant but also is able to tune plant growth and development according to the ever-changing external conditions surrounding the plant. In the meristems, auxin regulates cell division, elongation, and differentiation leading to downstream organogenesis that shapes shoot and root architecture. The vital roles of auxin gradients in plant growth and development have been established and interpreted mainly as the product of the combined action of auxin transport, signaling and response. Conversely, little is known about the contribution of the *de novo* auxin biosynthesis to the generation and maintenance of the morphogenic auxin maxima. A thorough understanding of how and where auxin is produced is nonetheless critical to our ability to precisely define auxin sources and sinks and thereby to establish a more refined picture of the polar transport system and auxin activity. It is only in the past 20 years that a combination of genetic, biochemical, and pharmacological approaches (Zhao et al., 2001; Cheng et al., 2006; Cheng et al., 2007; Stepanova et al., 2008; Tao et al., 2008; Mashiguchi et al., 2011; Stepanova et al., 2011), together with the development of more sensitive methodologies for auxin metabolite quantification (Novák et al., 2012), have led to the identification of the first complete pathway of auxin biosynthesis in plants. The best characterized auxin in plants, indole-3-acetic acid (IAA), is predominantly produced from the aromatic amino acid L-tryptophan (Trp) via indole-3-pyruvic acid (IPyA) in a two-step pathway (reviewed in Brumos et al., 2014). Trp is first converted to IPyA by a small family of tryptophan aminotransferases that in *Arabidopsis* is represented by TRYPTOPHAN AMINOTRANSFERASE OF ARABIDOPSIS1 (TAA1) (also known as WEAK ETHYLENE INSENSITIVE8 [WEI8] [Stepanova et al., 2008], SHADE AVOIDANCE3 [SAV3] [Tao et al., 2008], TRANSPORT INHIBITOR RESPONSE2 [TIR2] [Yamada et al., 2009], and CYTOKININ INDUCED ROOT CURLING1 [CKRC1] [Zhou et al., 2011]) and its paralogs TRYPTOPHAN AMINOTRANSFERASE RELATED1 (TAR1) and TAR2 (Stepanova et al., 2008). IPyA is then converted into IAA by the YUCCA (YUC) family of flavin monooxygenases that in *Arabidopsis* consists of 11 members, YUC1 through YUC11 (reviewed in Zhao, 2014).

According to the classical view in the auxin field, a majority of auxin in plants is produced in the shoot apical meristems, young leaves, and flower buds and is rapidly distributed throughout the plant via the phloem (reviewed in Teale et al., 2006). In addition, auxin can move more slowly cell to cell via polar auxin transport with the help of auxin influx carriers AUXIN1 (AUX1)/LIKE-AUXs (LAXs) and auxin efflux transporters PIN FORMED (PINs) and ABCB/MULTIDRUG RESISTANCE (MDR)/PHOSPHOGLYCOPROTEIN (PGPs) (reviewed in Adamowski and Friml, 2015). It is the polar distribution of PINs within cells that is thought to enable directional flow of auxin to generate robust morphogenic auxin gradients that instruct plant development. The classical view has however been challenged by the finding that auxin can also be synthesized locally in roots (Ljung et al., 2002; Ljung et al., 2005; Stepanova et al., 2008). Cloning of the auxin biosynthesis genes *WEI8/TARs* and *YUC*s uncovered that they are expressed not only in shoots but also in roots, and the domains of expression of several of these genes coincide with the auxin response maxima in root tips (Stepanova et al., 2008; Chen et al., 2014), as defined by the auxin activity reporters *DR5:GFP* or *DII-VENUS* (Ulmasov et al., 1997; Brunoud et al., 2012; Liao et al., 2015). Multiple

higher order *wei8/tar* and *yuc* mutants show dramatic developmental effects (Stepanova et al., 2008; Tao et al., 2008; Cheng et al., 2007; Cheng et al., 2006), suggesting that local activity of the biosynthesis genes may have a direct role in the generation and/or maintenance of auxin maxima. Supporting the key role of local biosynthesis is the finding that auxin produced in the aerial parts of plants is unable to compensate for an auxin biosynthesis deficiency of *yucQ* mutants in roots, resulting in the degeneration of root meristems (Chen et al., 2014).

The discovery of an essential contribution of locally made auxin to PIN polarization and to the establishment of the apical-basal axis in young embryos further implicates tissue-specific auxin production in the control of plant development (Robert et al., 2013). Thus, in some developmental contexts, the location of auxin sources is of critical physiological importance, and long-distance transport may not suffice for the generation of morphogenetic auxin gradients in all tissues. On the other hand, a uniform supply of IAA in the growth medium can partially suppress the root meristem defects of strong auxin biosynthetic mutants (Stepanova et al., 2011), suggesting that a non-localized source of auxin readily available to roots may be all that is needed for the transport machinery to generate the auxin maxima required for root development. Consistent with the latter argument are the conclusions of the first experimental and mathematical modeling approaches that showed how the auxin transport system alone could generate robust auxin gradients in roots with any (i.e., non-local) sources of auxin (Grieneisen et al., 2007). Alternative models were later built under the assumption that minor production and degradation of auxin do take place in every root cell, but higher auxin production rates occur in the quiescent center (QC) and columella initials to account for the local synthesis of auxin in the root meristem (Band et al., 2014). If locally made auxin was removed from these models, the gradient was not qualitatively affected (Band et al., 2014), arguing against the crucial role of local sources of auxin. These modeling experiments, however, made an assumption that all root cells make some auxin, which is not in agreement with the highly restricted expression patterns of the *WEI8/TAR* family in roots (Stepanova et al., 2008). Thus, the relative contributions of local auxin production and transport, both long and short distance, remain largely undefined, warranting the need for further inquiry into the potentially overlapping roles of the biosynthesis and transport of this hormone.

Both auxin biosynthesis and transport regulate plant development not only under optimal laboratory conditions but also in response to a stress hormone ethylene (Růzicka et al., 2007; Swarup et al., 2007; Stepanova et al., 2007; Stepanova et al., 2008). Exposure of plants to ethylene or its precursor ACC is known to trigger specific patterns of local auxin production, transport, and response in roots of *Arabidopsis* seedlings by stimulating transcription of auxin biosynthesis and transport genes (Růzicka et al., 2007; Swarup et al., 2007; Stepanova et al., 2007; Stepanova et al., 2008). Not surprisingly, genetic defects in the numerous components of the auxin biosynthesis, transport, perception, or response machineries (Merchante and Stepanova, 2017) lead to root-specific ethylene insensitivity. These findings suggest that auxin production and transport and, consequently, proper levels of auxin signaling and response are prerequisites for normal responses of *Arabidopsis* roots to ethylene and provide a convenient platform for elucidating the respective roles of auxin biosynthesis and transport in a physiologically relevant context.

Herein, we evaluated the contribution of localized auxin production versus polar transport to specific growth and development programs in *Arabidopsis*. Our data indicate that root-produced local sources of auxin are required for root stem cell niche maintenance, whereas shoot-derived auxin alone cannot keep the root meristems alive. Local auxin biosynthesis and auxin transport in roots act redundantly in the establishment and maintenance of robust morphogenetic maxima critical for root meristem activity. In contrast, local auxin biosynthesis is essential (and cannot be fully compensated for by transport) for root responses to hormone ethylene, as well as for flower development. Thus, local auxin production and transport in plants represent partially redundant physiological mechanisms that work together to confer greater robustness and tunability to instructional auxin gradients, enabling developmental plasticity and adaptation of plants to changing environmental conditions.

RESULTS AND DISCUSSION

Auxin Produced in the Root Is Required for Maintaining Functional Root Meristems

Prior studies (Stepanova et al., 2008) demonstrated that in *wei8 tar2* a deficiency in auxin synthesized via the IPyA pathway results in a loss of robust auxin gradients and leads to root meristem degeneration. Herein, to dissect the role of shoot- versus root-derived auxin in root meristem maintenance, we performed reciprocal grafting of shoots and roots of wild-type (WT) and *wei8 tar2* seedlings introgressed with an auxin-responsive reporter *DR5:GFP* at 3 days post germination, i.e., prior to mutant seedlings displaying any obvious signs of root stem cell loss (Stepanova et al., 2008), and examined *DR5:GFP* activity 1 week and 3 weeks after the surgery (Figures 1A and S1A). WT shoots grafted onto the mutant roots (WT/*wei8 tar2*) did not prevent root meristem degeneration, suggesting that WT shoot sources of auxin could not compensate for the auxin deficiency in roots and that auxin produced locally in roots is critical for root meristem health. One can argue that in these plants the vasculature may reconnect too late for the shoot-derived auxin to reach the root tip on time and prevent *wei8 tar2* root meristem degeneration. Indeed, although the phloem of grafted WT plants reconnects within 3 days of grafting (Melnyk et al., 2015), the process may take longer in grafts involving the compromised *wei8 tar2* vasculature, and the meristematic potential of *wei8 tar2* roots does decline over time (see below). Nonetheless, WT roots that received mutant shoots (*wei8 tar2*/WT) maintained healthy root meristems with normal patterns of *DR5:GFP* (Figure 1A), implying that local supply of auxin is necessary for root stem cell niche maintenance. One caveat of this experiment is that the shoots of *wei8 tar2* are not completely devoid of auxin (Stepanova et al., 2008), and thus, the possibility that in these grafted plants some shoot auxin did travel to the roots cannot be discarded. On the other hand, auxin locally produced in WT roots of *wei8 tar2*/WT grafted plants was not sufficient to reverse the morphological defects of *wei8 tar2* shoots (Figure S1B). Control experiments

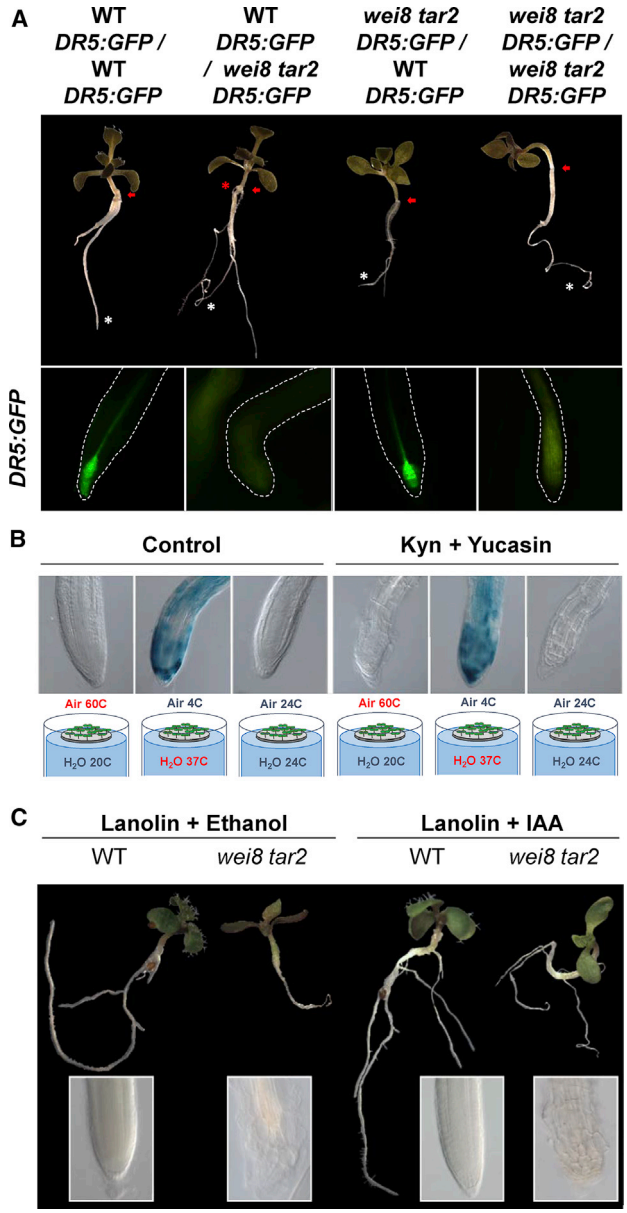

Figure 1. Local Auxin Production in the Root Is Required for Root Meristem Maintenance

(A) Reciprocal grafting of auxin-deficient *wei8 tar2* and WT Columbia seedlings that harbor an auxin responsive reporter *DR5:GFP* was performed in 3-day-old plants. Representative 10-day-old grafted seedlings and root *DR5:GFP* patterns in these plants are displayed. Red arrows mark the sites of grafting. White asterisks label primary roots, and red asterisks indicate adventitious roots. Dotted lines delineate the contour of each root.

(B) 3-day-old seedlings harboring a heat shock-inducible Cre/Lox bacterial auxin production system were germinated in the absence (control) or presence of the IPyA-pathway inhibitors (Kynurenine and Yucasin) and subjected to local heat application to activate auxin production specifically in roots or shoots. Activation of the system was monitored by GUS staining. Roots of 10-day-old seedlings are shown.

(C) Lanolin paste supplemented with auxin (IAA) or solvent (ethanol) was applied to the shoot apexes of *wei8 tar2* and WT seedlings 3 days and again 6 days after germination. Representative 14-day-old seedlings and their primary root meristems are shown.

See also Figure S1.

with WT/WT grafts resulted in normal *DR5:GFP* expression in roots, whereas *wei8 tar2/wei8 tar2* grafts lost their *DR5:GFP* and root meristem activity (Figure 1A). Additional controls using detached roots showed root degeneration and loss of *DR5:GFP* activity (Figure S1A). These results are consistent with the notion that local auxin produced in roots is required for root meristem activity. Likewise, shoots but not necessarily shoot-derived auxin are needed for root survival.

To differentiate between the roles of shoot versus root sources of auxin in root meristem maintenance, we next employed a heat shock-inducible Cre/Lox auxin production system (Figure S1C) (Dubrovsky et al., 2008). This system turns on a bacterial auxin biosynthesis enzyme, iaaM, upon exposure of plants to heat stress, and the activation of the system can be monitored by GUS staining. We amended the system by introducing another bacterial auxin biosynthesis gene, *iaaH*, into the plants that harbor the *Cre>>iaaM/GUS* system to insure rapid and efficient auxin production independent of the endogenous plant pathways (Figure S1C). We triggered auxin synthesis in shoots or in roots by exposing the above- or below-ground parts of seedlings to high temperatures and monitored the effectiveness of the treatment by relying on GUS activity (Figures 1B and S1D). To eliminate the effect of the major endogenous pathway of auxin biosynthesis, we applied a combination of kynurenine (an inhibitor of TAA1/TARs) and yucasin (an inhibitor of YUCs) to block the IPyA route of auxin biosynthesis and to ensure that most if not all auxin in the heat-treated plants is made via the transgenic bacterial iaaM/iaaH pathway (Figure 1B). In the presence of the inhibitors, the roots of transgenic plants that received no heat shock or had auxin biosynthesis induced only in the aerial parts, like WT plants receiving the root heat shock but not harboring the auxin inducible system, lost their root meristematic activity and degenerated, whereas the heat-treated roots of transgenic plants retained healthy meristems (Figures 1B and S1D). Thus, shoot-derived auxin alone cannot support the root stem cell niche, and root sources of auxin are critical for maintaining the root meristem identity, consistent with prior findings (Chen et al., 2014).

Next, we applied exogenous IAA to the shoots of *wei8 tar2* seedlings and examined the fate of the root meristems (Figure 1C). Unlike mock-treated plants, double mutants treated on the shoot with IAA formed several lateral and adventitious roots (Figures 1C and S1E), indicating that externally supplied auxin did move down the hypocotyl and the root. Nonetheless, the primary root meristems of plants treated with IAA on the shoot lost their stem cell identity and differentiated (Figure 1C) despite repeated application of IAA. Importantly, not only the primary roots but also the later emerging lateral and adventitious root meristems degenerated (Figures 1C and S1E), again confirming that auxin production in the root is necessary for supporting a healthy root meristem and that shoot-derived auxin, although capable of inducing new roots, is not sufficient to keep root stem cells functional. Thus, the long-distance phloem-based auxin transport from the shoot previously implicated in adventitious and lateral root emergence (Swarup et al., 2008; Overvoorde et al., 2010) and root growth (Fu and Harberd, 2003) may not be a critical player in the generation and maintenance of a local auxin maximum in the root meristem.

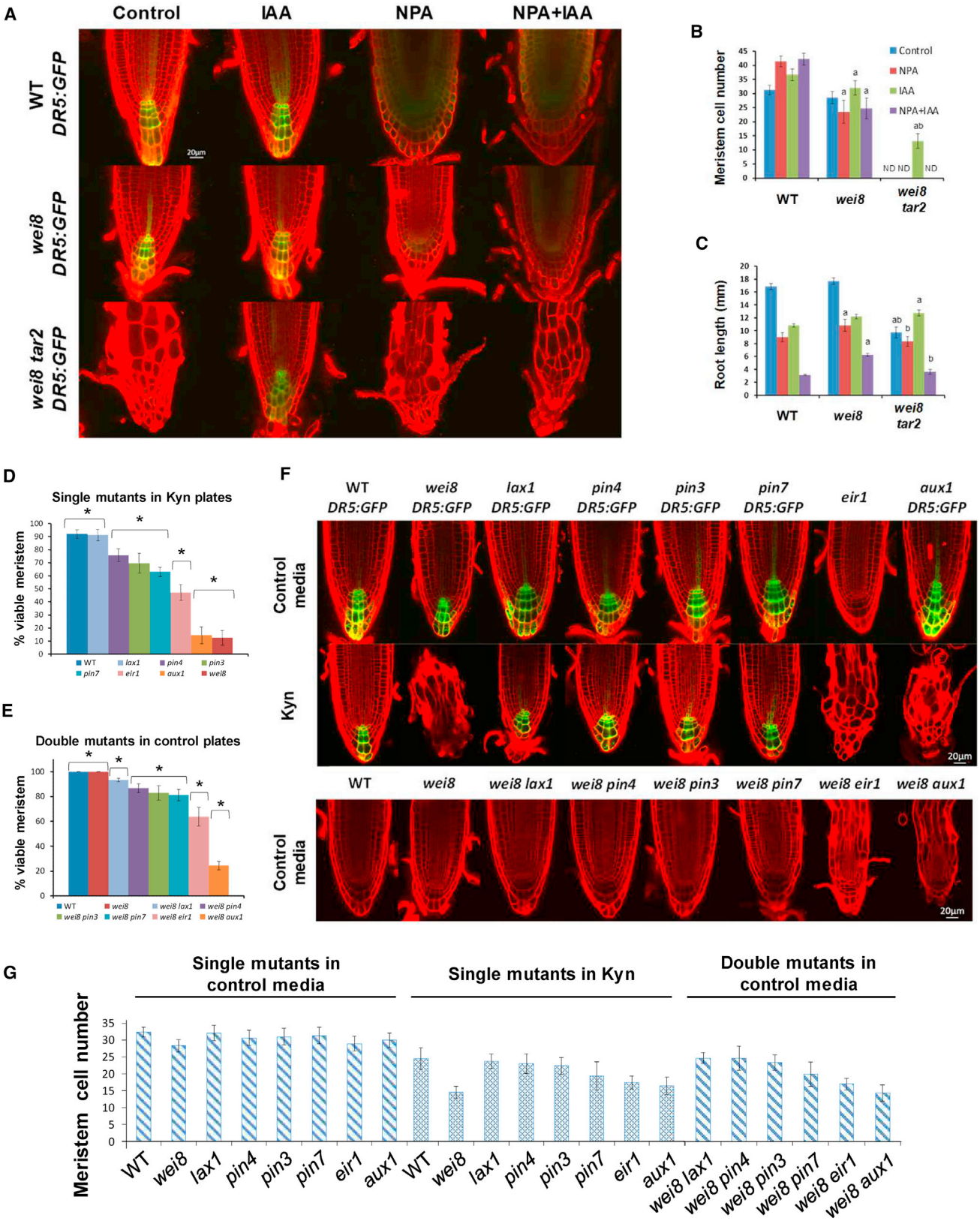

(legend on next page)

Auxin Biosynthesis and Transport Play Overlapping Roles in Root Meristem Maintenance

Root meristems of *wei8 tar2* grown in media supplemented with IAA do not degenerate (Figure 2A) (Stepanova et al., 2011), indicating that a uniform auxin supply to the root is capable of keeping the mutant root meristems alive. Partial restoration of the stem cell niche structure is observed (Figures 2A and S2A), with about half the number of meristem cells in the complemented *wei8 tar2* roots relative to WT meristems (Figure 2B), leading to partial root growth recovery of the double mutant in auxin (Figure 2C). A high incidence of *wei8 tar2* root meristem survival is witnessed not only in seedlings directly germinated in IAA but also in plants that are transferred to IAA plates 3 days after sowing (with over 90% of double mutants preserving a stem cell niche) (Figure S2B). The recovery rates, however, drop if seedlings are moved to auxin-supplemented media at later stages, with only a 10% recovery rate seen in 7-day-old plants (Figure S2B), suggesting that in the absence of available auxin, the root meristems of *wei8 tar2* degenerate irreversibly over time, consistent with our prior observations (Stepanova et al., 2008). These findings also imply that as long as root tips have direct access to a source of IAA, auxin transporters alone can generate an auxin maximum in the meristem to support root stem cell activity and root growth, as postulated previously (Grieneisen et al., 2007; Band et al., 2014).

We next tested the effect of a polar auxin transport inhibitor *N*-1-naphthylphthalamic acid (NPA) (that blocks auxin efflux by interfering with the activity of PIN and MDR/PGP transporters) (Blakeslee et al., 2007; Geisler et al., 2005) on the root meristem health of WT and mutant seedlings (Figures 2A–2C and S2A). WT plants germinated in the presence of NPA for 10 days exhibit root meristems that, although morphologically altered (Figures 2A–2C), retain their meristematic potential, as upon transfer to control media, they recover normal cell niche structure and *DR5:GFP* activity patterns (Figure S2C). This suggests that in plants treated with NPA, i.e., when the polar auxin transport system has been perturbed, auxin biosynthesis alone can keep the root meristems alive. In contrast, if both auxin biosynthesis and auxin transport are compromised, as in NPA-treated *wei8 tar2*, exogenous application of IAA can no longer revert the mutant defects and preserve a functional root meristem, resulting in stem cell loss and root degeneration (Figures 2A–2C and S2A). These results are consistent with the notion that local auxin biosynthesis and polar transport in roots play cooperative and somewhat redundant roles in maintaining a robust root meristem. The two mechanisms can also support stem cell function individually, but when both are eliminated simultaneously, root degeneration occurs even in the presence of an abundant uniform source of auxin. This conclusion is in line with the observation that *wei8* single mutants are hypersensitive to NPA (Figures 2A–2C, S2A, and S2D). Nonetheless, 70% of 18-day-old NPA-grown *wei8* mutants maintained viable root meristems despite having reduced levels of auxin biosynthesis (as a result of the loss of *WEI8*) and blocked auxin transport (as a consequence of the NPA treatment) (Figure S2D). These observations suggest that in the absence of *WEI8*, the activity of other auxin biosynthetic genes in the root meristem is sufficient, even when auxin transport is perturbed, to generate a robust enough maximum of auxin to preserve the root meristem potential. In fact, translational fusions with *GUS* show that the NPA treatment upregulates the levels of an otherwise poorly expressed *WEI8* paralog *TAR2* and of at least one of the downstream root-expressed *YUC* genes, *YUC3* (Figure S2E). This altered expression of auxin biosynthetic genes triggered by NPA implies that some of the changes caused by blocking auxin transport may not necessarily stem from the direct impact of NPA on auxin transport but from its effects on altering the levels and/or patterns of local auxin biosynthesis.

We also evaluated the role of auxin import in root meristem maintenance by utilizing 1-naphthoxyacetic acid (1-NOA), an inhibitor of auxin influx carriers, and the synthetic auxin NAA that can enter plant cells via diffusion but requires active efflux carriers (PINs and/or MDR/PGPs) for cell-to-cell transport (Delbarre et al., 1996). NAA does not enter the AUX1-dependent shootward flux and accumulates in the root cap (Band et al., 2014), thus resulting in a noticeable broadening of the *DR5:GFP* domains in root meristems (Figure S2F). Treatment with NAA, like that with IAA, complements the root meristem degeneration defect of *wei8 tar2* and partially restores *DR5:GFP* patterns (Figure S2F), suggesting that in these plants, auxin efflux carriers

Figure 2. Local Auxin Biosynthesis and Auxin Transport Are Individually Capable of Maintaining Viable Root Meristems

(A) WT, *wei8*, and *wei8 tar2* seedlings harboring *DR5:GFP* were germinated in control media or in media supplemented with 100-nM IAA, 10-μM NPA, and a combination of both additives for 10 days. Representative root confocal microscope images are displayed. Propidium iodide staining is shown in red, and the activity of *DR5:GFP* is seen in green.

(B) Root meristem cell number was quantified in 10-day-old WT, *wei8*, and *wei8 tar2* seedlings grown in control media and in media supplemented with NPA, IAA, or both, as in (A) ($n \geq 25$ roots). Letters mark significant differences ($p < 0.01$) in response to the same treatment between a mutant and WT (a) or between two mutants (b). ND, not detected, as *wei8 tar2* displays fully degenerated root meristems.

(C) Root lengths were quantified in 10-day-old WT, *wei8*, and *wei8 tar2* seedlings grown in control media and media supplemented with NPA, IAA, or both, as in (A) ($n \geq 30$ roots). Letters mark significant differences ($p < 0.01$) in response to the same treatment between a mutant and WT (a) or between two mutants (b).

(D) Primary root meristem viability was quantified in WT, *wei8*, and single auxin transporter mutants in the presence of 1-μM L-Kynurenine ($n \geq 80$ roots). Genotypes that are not significantly different from one another are grouped under the same bracket, with asterisks indicating statistically different genotype groups; $p < 0.05$. Bars represent the means of the three percentages ± SD.

(E) Primary root meristem viability was quantified in WT, *wei8*, and double mutants of *wei8* with auxin transporters in control media ($n \geq 80$ roots). Genotypes that are not significantly different from one another are grouped under the same bracket, with asterisks indicating statistically different genotype groups; $p < 0.05$. Bars represent the means of the three percentages ± SD.

(F) Seedlings were germinated for 10 days in control media or in media supplemented with 1-μM L-Kynurenine. Confocal microscope images of representative primary root meristems are shown. Propidium iodide staining marks cells in red, and the activity of *DR5:GFP* is visible in green.

(G) Root meristem cell number of 10-day-old WT, *wei8*, single auxin transporter mutants grown in either control media or media supplemented with 1-μM L-Kynurenine, and double mutants grown in control media was quantified ($n \geq 30$ roots). Statistical analysis is shown in Figure S2H.

See also Figure S2.

alone could make a robust auxin maximum out of NAA that diffused into roots from the media. These observations are consistent with the notion that efflux carriers control the direction of auxin transport, but influx carriers fine-tune the sites of auxin accumulation (Band et al., 2014). To test the contribution of the influx carriers AUX1 and LAXs to establishing auxin maxima and root meristem function, we evaluated the effect of 1-NOA in plants lacking robust local sources of auxin, i.e., in *wei8 tar2* mutants grown in the presence of exogenous IAA. Importantly, 1-NOA treatment abolished the IAA-mediated complementation of the root meristem defect of *wei8 tar2* (Figure S2F), highlighting the critical role of auxin influx carriers in the accumulation of auxin maximum in the stem cell niche of the root. 1-NOA treatment of WT plants and *wei8* single mutants reduced the levels of *DR5*:*GFP* and modified the root meristem morphology but did not disrupt the viability of these root meristems (Figure S2F). Taken together, our findings reinforce the notion of the cooperative roles of auxin biosynthesis and transport in root stem cell activity and demonstrate the resilience of the mechanism maintaining the meristematic potential of the stem cell niche.

To corroborate the results of auxin transport inhibition obtained by pharmacological means with NPA and 1-NOA, we also evaluated the root stem cell activity of auxin transport mutants in the absence and presence of the WEI8/TAR inhibitor kynurenine (Figures 2D–2G, S2G, and S2H). While in control media all genotypes possessed healthy meristems, *pin3*, *pin4*, and *pin7* had a greater percentage of seedlings with degenerated meristems in kynurenine relative to WT and *lax1* (25%–-40% of the *pin* meristems are lost in kynurenine compared to just 10% in WT and *lax1*), *eir1*/*pin2* displayed a more dramatic kynurenine hypersensitivity (53% loss), and *aux1* showed severe root stem cell loss (86% loss) that is comparable to that of *wei8* itself (88%) (Figures 2D, 2F, 2G, and S2H). Furthermore, this gradation of defects was largely mirrored in the double mutant combinations between *wei8* and auxin transport mutants grown in control media without any supplements: *wei8 aux1* > *wei8 eir1* > *wei8 pin3* = *wei8 pin4* = *wei8 pin7* > *wei8* lax1 > wei8 = WT, with even *wei8 lax1* showing mild but discernable meristem defects (8% meristem loss) (Figures 2E–2G and S2H). The hypersensitivity of auxin transport mutants to the auxin biosynthesis inhibitor kynurenine and the synergistic interactions of the mutants that combine mild defects in both processes further argue in support of auxin transport and biosynthesis in roots working in concert with one another to ensure the health of the root meristems.

Local Auxin Biosynthesis in the Root Quiescent Center Is Required and Sufficient for Root Meristem Function When Auxin Transport Is Blocked

To determine where in the root auxin biosynthesis needs to take place to support stem cell function, we manipulated the patterns of expression of *WEI8*, the predominant member of the *WEI8/TAR* family, in the *wei8 tar2* mutant background. Since *tar2* single mutants do not show any prominent phenotypic defects (Stepanova et al., 2008), restoration of the *WEI8* activity in specific tissues of *wei8 tar2* is expected to bring back WT morphology in these tissues. Our earlier studies employing a large translational reporter construct made by recombineering in a context of a bacterial artificial chromosome, *WEI8p*$_{(TAC)}$*:GFP-WEI8*$_{TAC}$ (Stepanova et al., 2008) (Figure S3A), demonstrated that in roots, the reporter is highly active in the QC, is mildly expressed in the root vasculature and the epidermis of the root elongation zone, and is inducible by ethylene in the root epidermis (Stepanova et al., 2008). In contrast, another published *WEI8* construct, a translational fusion of its cDNA with *GUS* (3.4 Kb of the *WEI8* promoter, a full-length *WEI8* CDS without introns, fused to *GUS* in the C terminus, *WEI8p*$_{(3.4)}$*:WEI8*$_{cDNA}$*-GUS* [Yamada et al., 2009]) (Figure S3A), was described to lack QC-specific expression in roots and display a more uniform pattern of activity in root tissues above the QC. Importantly, both constructs have originally been demonstrated to revert the mild auxin-deficient phenotypes of *wei8* single mutants (Stepanova et al., 2008; Yamada et al., 2009).

To pinpoint what differentiates the patterns of expression and the complementation ability of the two reporters, we generated two new *WEI8* constructs by means of bacterial recombineering (Alonso and Stepanova, 2015). The new reporters, *WEI8p:YPet-WEI8*$_{gDNA}$ and *WEI8p:YPet-WEI8*$_{cDNA}$, harbor 10 Kb of the promoter (upstream of the start codon) and 5 kb of the downstream sequence (downstream of the stop codon) of *WEI8*, a full *WEI8* CDS with or without all introns, respectively, and a *YPet* fluorescent protein coding sequence in the N terminus (Figure S3B). The two transgenes showed contrasting domains of root activity, with the gDNA reporter displaying predominantly QC-specific expression and the cDNA construct being active in the epidermis of the root transition and elongation zones (Figure S3C). The only structural or sequence difference that sets the two new constructs apart is the presence versus absence of the introns (Figure S3B). Thus, the introns of *WEI8* contain critical regulatory elements that drive the expression of *WEI8* in the QC and restrict its activity in other parts of the root (Figure 3A). This finding has provided an essential genetic tool to restore or eliminate *WEI8* expression in the QC and thus to evaluate the functional implications of the QC-derived auxin for the root stem cell niche maintenance and root development. While both *WEI8p:YPet-WEI8*$_{gDNA}$ and *WEI8p:YPet-WEI8*$_{cDNA}$ could revert the root meristem degeneration of *wei8 tar2* in control media, in the presence of NPA, only the QC-expressed gDNA construct was able to do so (Figures 3A and S3D). These results can be interpreted as a requirement for local auxin production in the QC for root stem cell function in plants that are compromised in auxin transport, but in the presence of an active auxin transport machinery, this tissue-specific requirement is lifted.

To assess if QC-specific expression of *WEI8* is sufficient for root meristem activity in the absence of operational polar auxin transport, we expressed *WEI8* cDNA in *wei8 tar2* under the control of the *WOX5* promoter, a well-characterized QC marker (Sarkar et al., 2007) (Figure 3B). We also drove *WEI8* cDNA under an epidermis-specific *WER* (Lee and Schiefelbein, 1999) and ubiquitous *UBQ10* (Norris et al., 1993) promoters (Bao et al., 2014) (Figure 3B). All three constructs reverted the meristem degeneration defect of the mutant in unsupplemented media (Figure 3B, upper panels), suggesting that they lead to the root production of auxin that can either directly or upon the redistribution by the auxin transport machinery, generate robust auxin maxima. In media supplemented with NPA, *WOX5p*-driven *WEI8* could still support a functional meristem in *wei8 tar2* (Figures 3B, bottom panels, and S3E), indicating that QC-specific expression of *WEI8* and, accordingly, QC-restricted production of auxin is

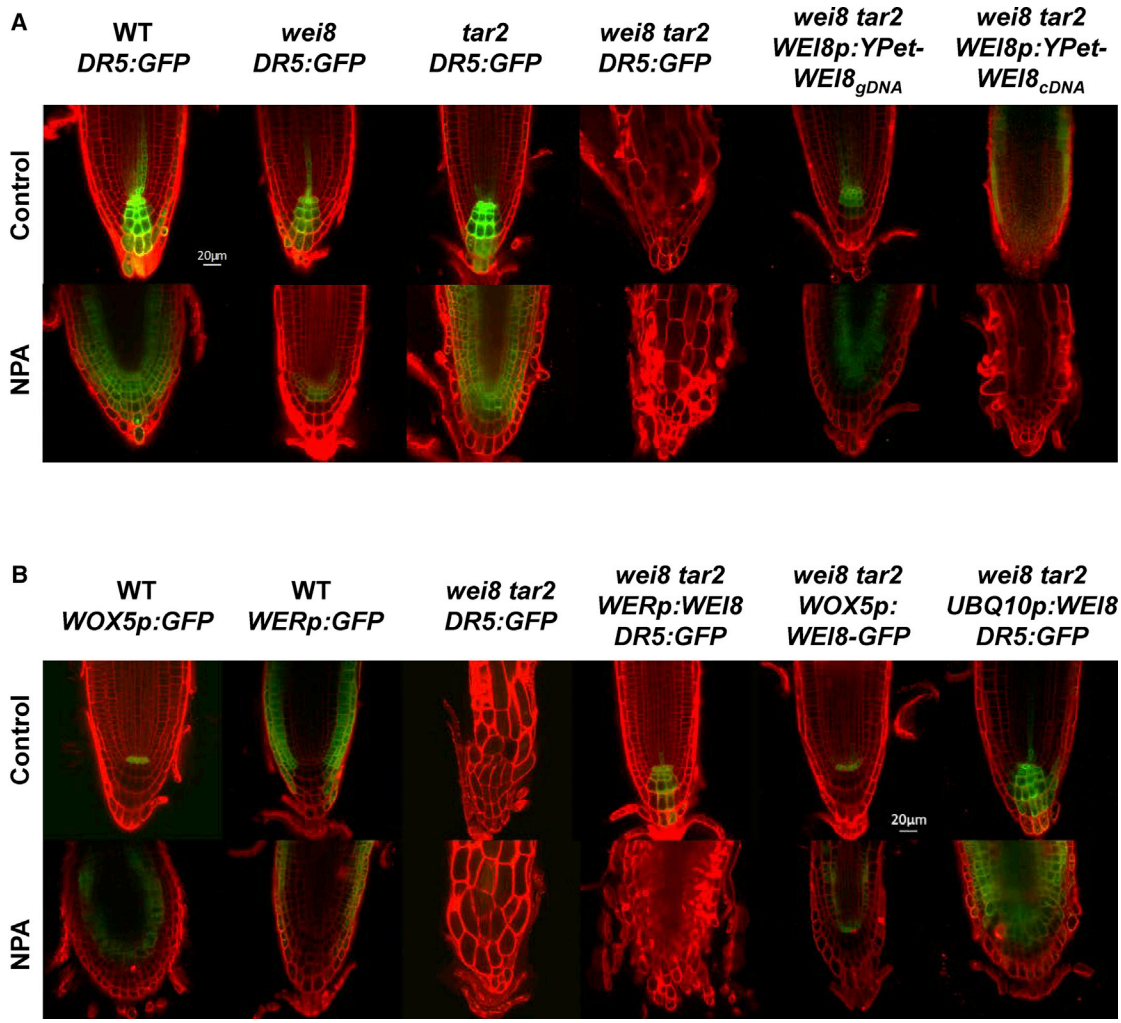

Figure 3. Local Auxin Biosynthesis in the Quiescent Center Is Required and Sufficient for Root Meristem Maintenance

(A) WT, *wei8*, *tar2, wei8 tar2 DR5:GFP*, *wei8 tar2* complemented with *WEI8p:YPet-WEI8*$_{gDNA}$, and *wei8 tar2* complemented with *WEI8p:YPet-WEI8*$_{cDNA}$ seedlings were germinated for 10 days in control media or in media supplemented with 10-μM NPA ($n \geq 75$ roots). Representative root meristems are shown. Propidium iodide staining is visible in red, and the expression of *DR5:GFP* or *YPet-WEI8* is seen in green.

(B) Seedlings of WT *WOX5p:GFP*, WT *WERp:GFP, wei8 tar2 DR5:GFP*, and *wei8 tar2* complemented with either *WERp:WEI8, WOX5p:WEI8-GFP*, or *UBQ10p:WEI8* were germinated for 10 days in control media or in media supplemented with 10-μM NPA ($n \geq 50$ roots). Representative root meristems are shown. Propidium iodide staining marks cells with red, and the expression of the GFP reporters is visible in green.

See also Figure S3.

sufficient for maintaining functional root meristems even when auxin efflux is compromised. *UBQ10p*-driven *WEI8* could also complement the root stem cell defect of *wei8 tar2* in NPA (Figures 3B, bottom panels, and S3E), suggesting that the restricted activity of the downstream *YUC* step of the auxin biosynthesis pathway (Figure S2E) can generate a maximum of auxin in the root meristem and support its stem cell identity. In contrast, in the presence of NPA, *WERp*-driven *WEI8* could not maintain a functional meristem in *wei8 tar2* (Figures 3B, bottom panels, and S3E). Thus, if IAA is produced and trapped in the epidermis, terminal stem cell differentiation occurs, highlighting the critical role of local QC-specific auxin biosynthesis for root stem cell activity in plants with a disrupted auxin transport system. Taken together, our results demonstrate that local auxin biosynthesis in the QC is both required and sufficient for root meristem maintenance in the absence of an operational polar auxin transport machinery. In unperturbed conditions, local auxin biosynthesis and local transport act in a coordinated manner to provide a resilient mechanism to maintain a robust root stem cell niche.

Precise Tissue-Specific Patterns of Auxin Biosynthesis Are Essential for Normal Responses of Roots to Ethylene

To assess the contribution of auxin production in response to environmental stresses, we tested the ability of the aforementioned *WEI8* constructs to complement the severe developmental defects of *wei8 tar2* in ethylene. Of the two previously published reporters, *WEI8p*$_{(TAC)}$*:GFP-WEI8*$_{TAC}$ and *WEI8p*$_{(3.4)}$*:WEI8*$_{cDNA}$*-GUS*, only the TAC construct could fully revert the

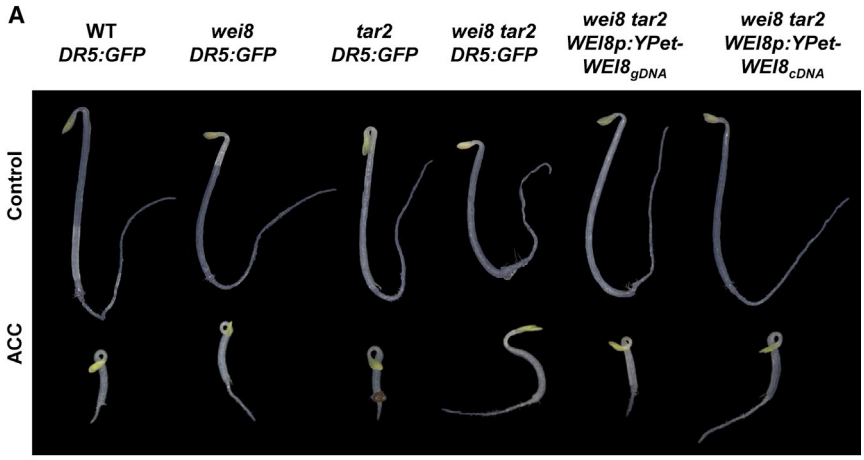

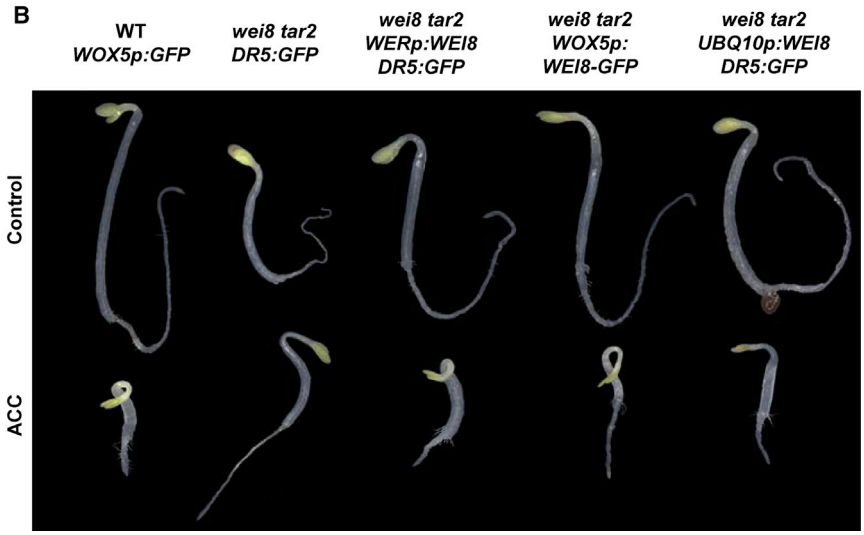

Figure 4. Proper Patterns of Local Auxin Biosynthesis in Roots Are Required for Root Sensitivity to Ethylene

(A) WT, *wei8*, *tar2*, *wei8 tar2 DR5:GFP*, *wei8 tar2* complemented with *WEI8p:YPet-WEI8*$_{gDNA}$, and *wei8 tar2* complemented with *WEI8p:YPet-WEI8*$_{cDNA}$ seedlings were germinated in the dark for 3 days in control media or in media supplemented with 10-μM ACC ($n \geq 80$ roots). Representative seedlings are shown.

(B) Seedlings of WT *WOX5p:GFP*, *wei8 tar2 DR5:GFP*, and *wei8 tar2* complemented with either *WERp:WEI8*, *WOX5p:WEI8-GFP*, or *UBQ10p:WEI8* seedlings were germinated in the dark for 3 days in control media or in media supplemented with 10-μM ACC ($n \geq 60$ roots). Representative seedlings are shown.

See also Figure S4.

insensitivity of *wei8 tar2* to ethylene (Stepanova et al., 2008) and its precursor 1-aminocyclopropane-1-carboxylic acid (ACC) (Figure S4A), whereas the cDNA construct could not restore the ACC responsiveness of the mutant roots but could revert the reduced ACC sensitivity in the apical hooks (Figure S4A). These observations confirm that the cDNA construct lacks some critical regulatory elements and that proper patterns or levels of *WEI8* expression are required for the root response to the stress hormone ethylene.

Consistent with these findings were also the results obtained with *WEI8p:YPet-WEI8*$_{gDNA}$ and *WEI8p:YPet-WEI8*$_{cDNA}$. Both reporters were induced by ACC, with the gDNA lines exhibiting expression in the root elongation zone and the cDNA lines showing expanded epidermal domains that spread into the upper root meristem but did not reach the QC (Figures S4B and S4C for ACC versus Figure S3C for control conditions), thus recapitulating the patterns described for the aforementioned original published constructs (Stepanova et al., 2008; Yamada et al., 2009) and exhibiting similar complementation capacity as the original constructs (Figures 4A and S4A) (Stepanova et al., 2008; Yamada et al., 2009). *WEI8p:YPet-WEI8*$_{gDNA}$ but not *WEI8p:YPet-WEI8*$_{cDNA}$ reverted the ACC insensitivity of *wei8 tar2* roots (Figures 4A and S4D), suggesting that proper patterns of *WEI8* expression and thus of auxin biosynthesis are critical for the ethylene response.

We also employed a *WEI8* gDNA construct with *GUS*, *WEI8p:GUS-WEI8*$_{gDNA}$ (Figure S4E) (Bhosale et al., 2018), and compared its expression patterns with that of the aforementioned *WEI8* cDNA line *tir2 WEI8p*$_{(3.4)}$*:WEI8*$_{cDNA}$*-GUS* (Yamada et al., 2009) (Figures S4F and S4G). In control media, the GUS activity of the two constructs was similar in the cotyledons and upper hypocotyls, but the relative intensity of the vasculature staining was greater in the cDNA than in gDNA lines. In the roots, the gDNA construct showed the characteristic QC expression, whereas the cDNA construct lacked expression in the QC but showed activity in the vasculature of the transition and elongation zone (Figure S4F). We did not observe epidermal staining in roots of 3-day-old *tir2 WEI8p*$_{(3.4)}$*: WEI8*$_{cDNA}$*-GUS* seedlings in control media, in contrast with what was reported for older light-grown plants (Yamada et al., 2009). Treatments with ACC induced expression of both the gDNA and cDNA constructs in shoots, leading to greater GUS staining on the inner (concave) side of the apical hooks and in the cotyledons (Figure S4F). In roots, *WEI8p:GUS-WEI8*$_{gDNA}$ displayed the expected (Figure S4C and Stepanova et al., 2008) ethylene-mediated induction in the elongation zone, whereas *WEI8p*$_{(3.4)}$*: WEI8*$_{cDNA}$*-GUS* in ACC showed staining in the root transition zone (Figure S4F). A prior study reported that *WEI8p*$_{(3.4)}$*: WEI8*$_{cDNA}$*-GUS* was sufficient to revert the mutant phenotype (NPA resistance) of *tir2/wei8* (Yamada et al., 2009). However, this construct failed to complement the ACC insensitivity of both *tir2* (Figures S4G and S4H) and *wei8 tar2* (Figure S4A), suggesting that the physiological requirements of plants for specific spatio-temporal patterns of auxin biosynthesis are different for the responses to different stimuli (NPA versus ethylene, in this case).

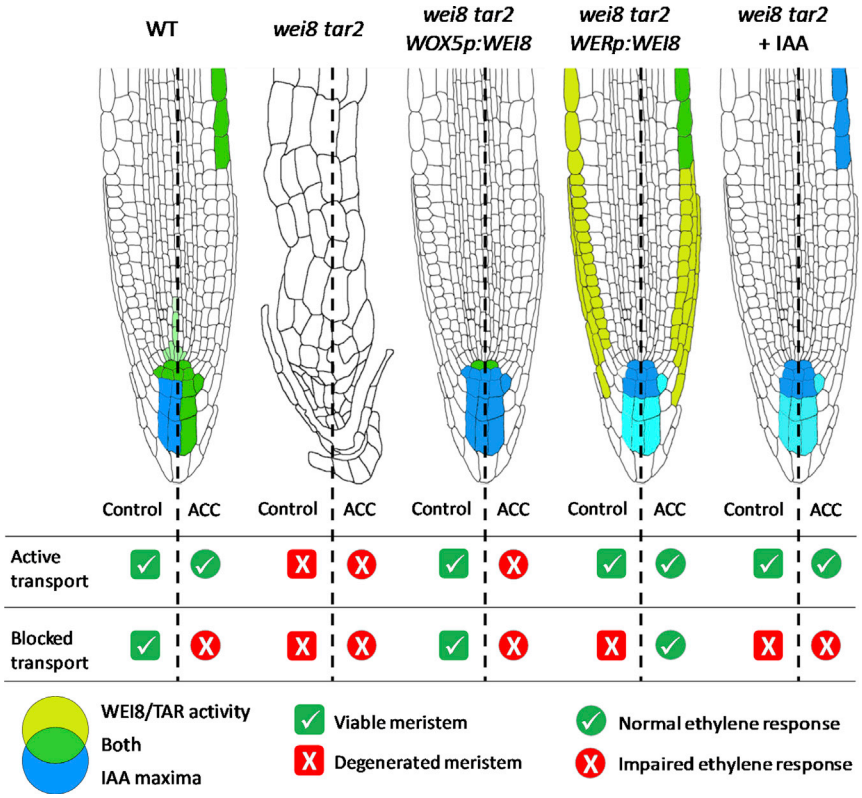

Figure 5. Schematic Model of the Roles of Local Auxin Biosynthesis in Root Development

Auxin transport and local biosynthesis work in concert to generate robust auxin maxima. IAA accumulation in the epidermis of the root elongation zone by means of local auxin production and/or active transport is required for triggering ethylene responses in roots. Auxin locally produced in the QC and/or delivered to the QC by the transporters is sufficient for maintaining viable root meristems. See main text for more details. Root tip schematics are shown. Yellow color marks the sites of WEI8/TAR activity, blue color highlights the sites of auxin accumulation, and green color shows where auxin biosynthesis and maxima coincide spatially. Each root is split by a dashed line into two halves, with the left side corresponding to control conditions and the right side reflecting what happens upon treating the plants with the ethylene precursor ACC. Check marks signify viable meristems (green squares) and normal ethylene responses (green circles). Cross marks label the loss of meristem activity (red squares) and compromised sensitivity to ethylene (red circles).

Prior studies demonstrated that ethylene promotes auxin production and transport in root tips leading to the formation of a second (besides QC) auxin response maximum in the root elongation zone (Růzicka et al., 2007; Swarup et al., 2007; Stepanova et al., 2007; Stepanova et al., 2008), sensitizing plant roots to ethylene. Activation of local auxin production is achieved by the precise ethylene-mediated induction of the IPyA pathway through the upregulation of *WEI8/TAR2* (Stepanova et al., 2008), several members of the *YUC* family (Liu et al., 2016), and of upstream tryptophan biosynthesis enzyme genes *WEI2* and *WEI7* (Stepanova et al., 2005) in specific cell types of the root. Consistently, the QC-specific expression of *WEI8* did not restore the response of *wei8 tar2* to ethylene, as seedlings expressing the *WEI8* cDNA under the *WOX5* promoter displayed long roots (Figures 4B and S4I) in the presence of ACC that efficiently inhibited root growth in control WT *WOX5p:GFP* plants with functional *WEI8* and *TAR2* (Figures 4B and S4I) In contrast, epidermis-specific and ubiquitous expression of *WEI8* driven by the *WER* and *UBQ10* promoters, respectively, was much more effective than *WOX5p:WEI8-GFP* at complementing the ethylene defects of the double mutant roots (Figures 4B and S4I). This suggests that the aforementioned boost in auxin biosynthesis in the epidermis of the root elongation zone in plants exposed to ethylene (Stepanova et al., 2007) is required for the normal root ethylene response. These observations are consistent with the recent report by Vaseva and co-authors that pinpointed root epidermis as the major site of ethylene-triggered root growth inhibition (Vaseva et al., 2018). The situation is, however, likely to be more complex, as the epidermis-localized expression of *WEI8p:YPet-WEI8*$_{cDNA}$ (Figures S4B and S4C) poorly complements the root ACC insensitivity of *wei8 tar2* (Figure 4A). Thus, precise timing and/or levels of auxin production in addition to its spatial pattern may also play an important role in the regulation of root ethylene responses.

Taking all of these observations together, we present a graphical model on the role of local auxin biosynthesis in roots (Figure 5) that summarizes the key findings described above. WT roots under control conditions display an auxin maximum in the meristem as a result of the synergistic activities of local auxin biosynthesis and transport. If seedlings are treated with an ethylene precursor ACC, root growth is arrested as a consequence of auxin accumulation in the elongation zone due to the local induction of auxin biosynthesis and transport toward this region of the root. If auxin transport is blocked, roots do not properly respond to ethylene (Pickett et al., 1990; Roman et al., 1995). *wei8 tar2* is compromised in auxin production, resulting in decreased ethylene sensitivity and root meristem degeneration shortly after seedling germination. Transgenic approaches relying on *WOX5p*- and *WERp*-driven *WEI8* in *wei8 tar2* indicate that in control conditions, IAA produced in the QC or in the root epidermis can support the root stem cell viability. If auxin transport is impaired, the QC-specific but not the epidermis-restricted activity of *WEI8* is able to keep the root meristems of *wei8 tar2* alive. In plants treated with ACC, epidermally made auxin but not QC-produced IAA can restore the full sensitivity of *wei8 tar2* to ethylene. Even if auxin transport is blocked, epidermal sources of auxin can restore the ethylene response of the mutant. Finally, exogenous application of IAA is effective at restoring the meristem viability and ethylene responsiveness of *wei8 tar2* but only if auxin transport is operational. Cumulatively, these findings highlight the collaborative roles of auxin transport and local production in regulating root growth

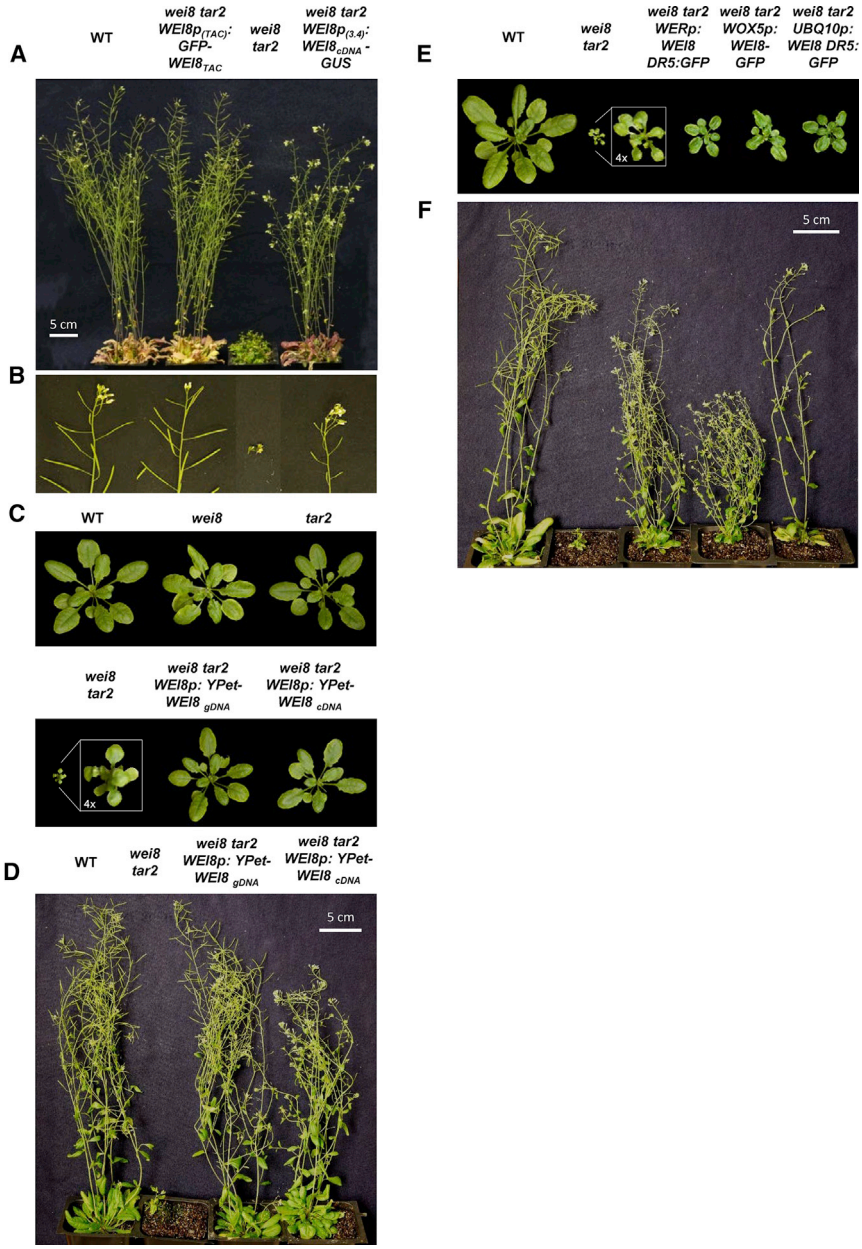

Figure 6. Proper Patterns of Auxin Biosynthesis Are Essential for Normal Plant Growth and Flower Development

(A and B) Adult phenotypes of soil-grown plants (A) or inflorescences (B) of WT Columbia, *wei8 tar2*, and *wei8 tar2* complemented with either $WEI8p_{(TAC)}$:*GFP-*$WEI8_{TAC}$ or $WEI8p_{(3.4)}$:$WEI8_{cDNA}$-*GUS* are displayed.

(C) Rosette phenotypes of soil-grown 4-week-old WT, *wei8*, *tar2, wei8 tar2*, and *wei8 tar2* complemented with either *WEI8p:YPet-*$WEI8_{gDNA}$ or *WEI8p:YPet-*$WEI8_{cDNA}$ are shown. Inlet provides a 4× image of *wei8 tar2*.

(D) Adult plants of soil-grown WT, *wei8 tar2, wei8 tar2* complemented with either *WEI8p:YPet-*$WEI8_{gDNA}$ or *WEI8p:YPet-*$WEI8_{cDNA}$ are portrayed.

(E) Rosette phenotypes of soil-grown 4-week-old WT, *wei8 tar2*, and *wei8 tar2* complemented with either *WERp:WEI8, WOX5p:WEI8-GFP* or *UBQ10p:WEI8* are displayed. Inlet provides a 4× image of *wei8 tar2*.

(F) Adult phenotypes of soil-grown WT, *wei8 tar2*, and *wei8 tar2* complemented with *either WERp: WEI8, WOX5p:WEI8-GFP* or *UBQ10p:WEI8* are portrayed. Representative plants are shown.

See also Figures S5 and S6.

both under control conditions and in the presence of the stress hormone ethylene.

Flower Fertility Requires Specific Spatiotemporal Patterns of Auxin Biosynthesis

Beyond its role in root stem cell function and ethylene sensitivity, auxin biosynthesis is essential for many other developmental processes. Accordingly, even partial auxin deficiency leads to profound phenotypic defects throughout the plant (Stepanova et al., 2008; Cheng et al., 2006; Cheng et al., 2007). Herein, we attempted to restore normal development in *wei8 tar2* by performing tissue-specific complementation with *WEI8*. We examined the ability of various *WEI8* constructs characterized above in root assays to revert the developmental defects of *wei8 tar2* in adult plants. While $WEI8p_{(TAC)}$:*GFP-*$WEI8_{TAC}$ (Stepanova et al., 2008) and $WEI8p_{(3.4)}$:$WEI8_{cDNA}$-*GUS* (Yamada et al., 2009) were both effective at complementing the rosette and inflorescence dwarfism of *wei8 tar2*, only the former was effective at restoring flower fertility (Figures 6A and 6B). $WEI8p_{(TAC)}$:*GFP-*$WEI8_{TAC}$ is expressed in the outer cell layers of early-stage flower buds and, upon establishment of the gynoecium, in the two well-defined cell files of the meristematic medial ridge (Stepanova et al., 2008). This is consistent with the GUS and YPet activity patterns observed for *WEI8p:GUS-*$WEI8_{gDNA}$ and *WEI8p:YPet-*$WEI8_{gDNA}$ flowers (Figures S5A and S5B, upper panels). In contrast, $WEI8p_{(3.4)}$:$WEI8_{cDNA}$-*GUS* and *WEI8p:YPet-*$WEI8_{cDNA}$ show expression in the stamens and the receptacle of mature flowers (Figures S5A and S5B, bottom panels). No reporter activity is observed for the two cDNA constructs in the outer L1 cell layers during early flower bud development, and reduced expression is detected in the gynoecium of the cDNA lines as compared to that for the two gDNA constructs (Figures S5A and S5B). Although both *WEI8p:YPet-*$WEI8_{gDNA}$ and *WEI8p:YPet-*$WEI8_{cDNA}$ constructs could rescue the severe growth retardation of *wei8 tar2* leaves and inflorescences (Figures 6C and 6D), only the gDNA construct could fully complement the mutant flower sterility (Figures 6D and S5C–S5F). While the flowers of cDNA-complemented lines, unlike those of untransformed *wei8 tar2*, appeared fairly normal morphologically and formed robust-looking male and female organs, the stamen filaments were shorter than those of WT flowers and often

displayed delayed anther dehiscence (Figures S5C–S5E). We could overcome the structural infertility caused by the short stamens with manual pollination, but the seed set of crosses that involved the cDNA-complemented line was still lower than that of gDNA-complemented double mutants, revealing both male and female fertility defects in reciprocal crosses (Figure S5F). We conclude that the differences in *WEI8* expression from the transgenes in the developing flowers of these cDNA versus gDNA lines (Figures S5A and S5B) that likely translate into different patterns and/or levels of auxin production lead to functional differences in these organs reflected in the sterility versus full fertility of the cDNA- and gDNA-complemented flowers, respectively.

We also evaluated the ability of the three tissue-specific constructs of *WEI8* to complement *wei8 tar2* in adults. *WOX5p*-, *WERp*-, and *UBQ10p*-driven *WEI8* partially restored the growth of the mutant rosettes and inflorescences (Figures 6E and 6F), but neither construct was able to revert the flower fertility defect of *wei8 tar2* (Figures 6F, S5G, and S5H), highlighting the strict requirement for proper patterns and/or levels of auxin biosynthesis in these organs for normal flower development. Based on public RNA sequencing (RNA-seq) data ([Klepikova et al., 2016], travadb.org), native *WOX5* and *WER* have little or no expression in developing flowers, and low to moderate expression in shoot meristems, young leaves, and developing siliques (Figure S6A). *UBQ10*, on the other hand, is strongly expressed in all of these organs at an overall level orders of magnitude higher than that of *WEI8* itself. In the gynoecium, which, based on public microarray (Waese and Provart, 2016; eFP Browser 2.0) and RNA-seq data (Klepikova et al., 2016; travadb.org), represents the organ with the highest level of endogenous *WEI8* expression in the aerial parts of an adult plant, *UBQ10* is expressed at a level 5-fold higher than that of endogenous *WEI8* (see carpels and stigma values in Figure S6A), yet *UBQ10p*-driven ectopically expressed *WEI8* is unable to revert the flower infertility of *wei8 tar2* (Figures 6F, S5G, and S5H). Thus, even if *UBQ10*p-driven *WEI8* can produce enough IPyA in the flowers, *YUC*s may not be able to restrict the production sites of auxin to where auxin transporters can then take it and properly redistribute, leading to the construct's inability to revert the sterility phenotype of *wei8 tar2*. These findings confirm that for normal flower development, not only the levels but also the spatiotemporal patterns of *WEI8* activity and, accordingly, of auxin biosynthesis are critical. In this developmental context, auxin transport alone is unable to create proper gradients of auxin, and local auxin biosynthesis is essential for the establishment of robust morphogenic auxin maxima. In contrast, overall plant growth, reflected in the complexity of cotyledon and leaf vasculature and the size of rosettes of the complemented *wei8 tar2* mutant lines is similar for *WOX5p*-, *WERp*-, and *UBQ10p*-driven transgenes (Figures 6E, 6F, S6B, and S6C), whereas the defects in general plant architecture correlate with the strength of the promoter driving *WEI8* (Figure S6A). These findings indicate that the spatial and temporal auxin requirements and the degree by which auxin transport can compensate for altered local patterns of auxin biosynthesis are very context dependent and thus affected by the plant tissue and/or developmental stage.

Taken together, our results show that local auxin biosynthesis cooperates with the auxin transport machinery to generate robust morphogenic auxin gradients under a variety of scenarios. Unlike root meristem maintenance where auxin production and transport play redundant roles, at least some developmental processes (such as flower development) and environmental interactions (such as responses of plants to the stress hormone ethylene) rely on the contribution of both local auxin production and transport to support normal plant development and enable adaptive phenotypic plasticity. Thus, in all of the developmental contexts and stress response scenarios examined in this study, the two machineries of auxin maxima generation, local biosynthesis and transport, act in concert to provide a reliable (although not always fail-safe) mechanism to achieve the desired auxin distribution patterns that, if needed, can be tweaked to enable plant adaptation (i.e., upon exposure to the stress hormone ethylene). Furthermore, although this study has focused exclusively on the role of local IPyA-dependent IAA production and transport, it is important to emphasize that additional routes of the biosynthesis of IAA and of other endogenous auxins, as well as auxin sequestration and metabolism (conjugation, release, and/or catabolism), and ultimately auxin perception and signaling likely also all contribute to the generation of auxin activity gradients that govern plant development.

STAR★METHODS

Detailed methods are provided in the online version of this paper and include the following:

- KEY RESOURCES TABLE
- CONTACT FOR REAGENT AND RESOURCE SHARING
- EXPERIMENTAL MODEL AND SUBJECT DETAILS
  - Strains and Genotyping
- METHOD DETAILS
  - Recombineering Translational Fusion Lines
  - Plant Growth Conditions and Physiological Assays
  - Microscopy
  - CryoSEM Imagining
  - Grafting
  - A Cre/Lox-Based System to Induce Local Auxin Biosynthesis
  - Auxin Applications to Apical Shoot
  - Tissue-Specific *WEI8* Expression Lines Using *WOX5*, *UBQ10*, and *WER* Promoters
- QUANTIFICATION AND STATISTICAL ANALYSIS

SUPPLEMENTAL INFORMATION

Supplemental Information includes six figures and two tables and can be found with this article online at https://doi.org/10.1016/j.devcel.2018.09.022.

ACKNOWLEDGMENTS

This work was supported by the NSF grants MCB0923727, IOS1444561, and IOS1650139 to J.M.A. and A.N.S.; MCB1158181 to J.M.A.; an REU supplement MCB1434905 to fund T.C.V. and S.J.; a summer REU internship to T.C.V. from DBI1558579; and a Spanish Ministerio de Educacion postdoctoral fellowship to J.B. We thank R. Franks and M. Rojas-Pierce and NCSU AIF and CMIF services for assistance with microscopy; K. Karrass and L. Brumos and E. Brumos for aid in figure preparation; and members of the Alonso-Stepanova lab for helpful comments and stimulating discussions.

AUTHOR CONTRIBUTIONS

J.B., J.M.A., and A.N.S. designed experiments, performed research, analyzed data, and wrote the manuscript. L.M.R. performed preliminary genetic and pharmacological analyses. J.Y. made recombineering lines. T.C.V. and S.J. assisted in genotyping.

DECLARATION OF INTERESTS

The authors declare no competing interests.

Received: May 17, 2018
Revised: August 16, 2018
Accepted: September 26, 2018
Published: October 25, 2018

SUPPORTING CITATIONS

The following references appear in the Supplemental Information: Friml et al., 2002 and Friml et al., 2003.

REFERENCES

Adamowski, M., and Friml, J. (2015). PIN-dependent auxin transport: action, regulation, and evolution. Plant Cell *27*, 20–32.

Alonso, J.M., and Stepanova, A.N. (2015). A recombineering-based gene tagging system for *Arabidopsis*. Methods Mol. Biol. *1227*, 233–243.

Alonso, J.M., and Stepanova, A.N. (2014). *Arabidopsis* transformation with large bacterial artificial chromosomes. Methods Mol. Biol. *1062*, 271–283.

Alonso, J.M., Stepanova, A.N., Leisse, T.J., Kim, C.J., Chen, H., Shinn, P., Stevenson, D.K., Zimmerman, J., Barajas, P., Cheuk, R., et al. (2003). Genome-wide insertional mutagenesis of *Arabidopsis thaliana*. Science *301*, 653–657.

Band, L.R., Wells, D.M., Fozard, J.A., Ghetiu, T., French, A.P., Pound, M.P., Wilson, M.H., Yu, L., Li, W., Hijazi, H.I., et al. (2014). Systems analysis of auxin transport in the *Arabidopsis* root apex. Plant Cell *26*, 862–875.

Bao, Y., Aggarwal, P., Robbins, N.E., Sturrock, C.J., Thompson, M.C., Tan, H.Q., Tham, C., Duan, L., Rodriguez, P.L., Vernoux, T., et al. (2014). Plant roots use a patterning mechanism to position lateral root branches toward available water. Proc. Natl. Acad. Sci. USA *111*, 9319–9324.

Blakeslee, J.J., Bandyopadhyay, A., Lee, O.R., Mravec, J., Titapiwatanakun, B., Sauer, M., Makam, S.N., Cheng, Y., Bouchard, R., Adamec, J., et al. (2007). Interactions among PIN-FORMED and P-glycoprotein auxin transporters in Arabidopsis. Plant Cell *19*, 131–147.

Blilou, I., Xu, J., Wildwater, M., Willemsen, V., Paponov, I., Friml, J., Heidstra, R., Aida, M., Palme, K., and Scheres, B. (2005). The PIN auxin efflux facilitator network controls growth and patterning in *Arabidopsis* roots. Nature *433*, 39–44.

Bhosale, R., Giri, J., Pandey, B.K., Giehl, R.F.H., Hartmann, A., Traini, R., Truskina, J., Leftley, N., Hanlon, M., Swarup, K., et al. (2018). A mechanistic framework for auxin dependent *Arabidopsis* root hair elongation to low external phosphate. Nat. Commun *9*, 1409.

Brumos, J., Alonso, J.M., and Stepanova, A.N. (2014). Genetic aspects of auxin biosynthesis and its regulation. Physiol. Plant *151*, 3–12.

Brunoud, G., Wells, D.M., Oliva, M., Larrieu, A., Mirabet, V., Burrow, A.H., Beeckman, T., Kepinski, S., Traas, J., Bennett, M.J., et al. (2012). A novel sensor to map auxin response and distribution at high spatio-temporal resolution. Nature *482*, 103–106.

Chen, Q., Dai, X., De-Paoli, H., Cheng, Y., Takebayashi, Y., Kasahara, H., Kamiya, Y., and Zhao, Y. (2014). Auxin overproduction in shoots cannot rescue auxin deficiencies in *Arabidopsis* roots. Plant Cell Physiol. *55*, 1072–1079.

Cheng, Y., Dai, X., and Zhao, Y. (2007). Auxin synthesized by the YUCCA flavin monooxygenases is essential for embryogenesis and leaf formation in *Arabidopsis*. Plant Cell *19*, 2430–2439.

Cheng, Y., Dai, X., and Zhao, Y. (2006). Auxin biosynthesis by the YUCCA flavin monooxygenases controls the formation of floral organs and vascular tissues in *Arabidopsis*. Genes Dev. *20*, 1790–1799.

de Luis Balaguer, M.A., Fisher, A.P., Clark, N.M., Fernandez-Espinosa, M.G., Möller, B.K., Weijers, D., Lohmann, J.U., Williams, C., Lorenzo, O., and Sozzani, R. (2017). Predicting gene regulatory networks by combining spatial and temporal gene expression data in *Arabidopsis* root stem cells. Proc. Natl. Acad. Sci. USA *114*, E7632–E7640.

Delbarre, A., Muller, P., Imhoff, V., and Guern, J. (1996). Comparison of mechanisms controlling uptake and accumulation of 2,4-dichlorophenoxy acetic acid, naphthalene-1-acetic acid, and indole-3-acetic acid in suspension-cultured tobacco cells. Planta *198*, 532–541.

Dinneny, J.R., Long, T.A., Wang, J.Y., Jung, J.W., Mace, D., Pointer, S., Barron, C., Brady, S.M., Schiefelbein, J., and Benfey, P.N. (2008). Cell identity mediates the response of *Arabidopsis* roots to abiotic stress. Science *320*, 942–945.

Dubrovsky, J.G., Sauer, M., Napsucialy-Mendivil, S., Ivanchenko, M.G., Friml, J., Shishkova, S., Celenza, J., and Benková, E. (2008). Auxin acts as a local morphogenetic trigger to specify lateral root founder cells. Proc. Natl. Acad. Sci. USA *105*, 8790–8794.

Friml, J., Wisniewska, J., Benková, E., Mendgen, K., and Palme, K. (2002). Lateral relocation of auxin efflux regulator AtPIN3 mediates tropism in Arabidopsis. Nature *415*, 806–809.

Friml, J., Vieten, A., Sauer, M., Weijers, D., Schwarz, H., Hamann, T., Offringa, R., and Jürgens, G. (2003). Efflux-dependent auxin gradients establish the apical-basal axis of *Arabidopsis*. Nature *426*, 147–153.

Fu, X., and Harberd, N.P. (2003). Auxin promotes *Arabidopsis* root growth by modulating gibberellin response. Nature *421*, 740–743.

Geisler, M., Blakeslee, J.J., Bouchard, R., Lee, O.R., Vincenzetti, V., Bandyopadhyay, A., Titapiwatanakun, B., Peer, W.A., Bailly, A., Richards, E.L., et al. (2005). Cellular efflux of auxin catalyzed by the Arabidopsis MDR/PGP transporter AtPGP1. Plant J. *44*, 179–194.

Grieneisen, V.A., Xu, J., Marée, A.F.M., Hogeweg, P., and Scheres, B. (2007). Auxin transport is sufficient to generate a maximum and gradient guiding root growth. Nature *449*, 1008–1013.

Heidstra, R., Welch, D., and Scheres, B. (2004). Mosaic analyses using marked activation and deletion clones dissect *Arabidopsis* SCARECROW action in asymmetric cell division. Genes Dev. *18*, 1964–1969.

Klepikova, A.V., Kasianov, A.S., Gerasimov, E.S., Logacheva, M.D., and Penin, A.A. (2016). A high resolution map of the *Arabidopsis thaliana* developmental transcriptome based on RNA-seq profiling. Plant J. *88*, 1058–1070.

Kurihara, D., Mizuta, Y., Sato, Y., and Higashiyama, T. (2015). ClearSee: a rapid optical clearing reagent for whole-plant fluorescence imaging. Development *142*, 4168–4179.

Lee, M.M., and Schiefelbein, J. (1999). Werewolf, a MYB-related protein in *Arabidopsis*, is a position-dependent regulator of epidermal cell patterning. Cell *99*, 473–483.

Liao, C.Y., Smet, W., Brunoud, G., Yoshida, S., Vernoux, T., and Weijers, D. (2015). Reporters for sensitive and quantitative measurement of auxin response. Nat. Methods *12*, 207–210.

Liu, G., Gao, S., Tian, H., Wu, W., Robert, H.S., and Ding, Z. (2016). Local transcriptional control of *YUCCA* regulates auxin promoted root-growth Inhibition in response to aluminium stress in *Arabidopsis*. PLoS Genet. *12*, e1006360.

Ljung, K., Hul, A.K., Kowalczyk, M., Marchant, A., Celenza, J., Cohen, J.D., and Sandberg, G. (2002). Biosynthesis, conjugation, catabolism and homeostasis of indole-3-acetic acid in *Arabidopsis thaliana*. Plant Mol. Biol. *50*, 309–332.

Ljung, K., Hull, A.K., Celenza, J., Yamada, M., Estelle, M., Normanly, J., and Sandberg, G. (2005). Sites and regulation of auxin biosynthesis in *Arabidopsis* roots. Plant Cell *17*, 1090–1104.

Mashiguchi, K., Tanaka, K., Sakai, T., Sugawara, S., Kawaide, H., Natsume, M., Hanada, A., Yaeno, T., Shirasu, K., Yao, H., et al. (2011). The main auxin biosynthesis pathway in *Arabidopsis*. Proc. Natl. Acad. Sci. USA *108*, 18512–18517.

Melnyk, C.W., Schuster, C., Leyser, O., and Meyerowitz, E.M. (2015). A developmental framework for graft formation and vascular reconnection in *Arabidopsis thaliana*. Curr. Biol. *25*, 1306–1318.

Merchante, C., and Stepanova, A.N. (2017). The triple response assay and its use to characterize ethylene mutants in Arabidopsis. Methods Mol. Biol. *1573*, 163–209.

Montgomery, D.C. (2012). Design and Analysis of Experiments, Eighth Edition (Wiley).

Nakagawa, T., Kurose, T., Hino, T., Tanaka, K., Kawamukai, M., Niwa, Y., Toyooka, K., Matsuoka, K., Jinbo, T., and Kimura, T. (2007). Development of series of gateway binary vectors, pGWBs, for realizing efficient construction of fusion genes for plant transformation. J. Biosci. Bioeng. *104*, 34–41.

Nishimura, T., Hayashi, K., Suzuki, H., Gyohda, A., Takaoka, C., Sakaguchi, Y., Matsumoto, S., Kasahara, H., Sakai, T., Kato, J., et al. (2014). Yucasin is a potent inhibitor of YUCCA, a key enzyme in auxin biosynthesis. Plant J. *77*, 352–366.

Norris, S.R., Meyer, S.E., and Callis, J. (1993). The intron of *Arabidopsis thaliana* polyubiquitin genes is conserved in location and is a quantitative determinant of chimeric gene expression. Plant Mol. Biol. *21*, 895–906.

Novák, O., Hényková, E., Sairanen, I., Kowalczyk, M., Pospíšil, T., and Ljung, K. (2012). Tissue-specific profiling of the *Arabidopsis thaliana* auxin metabolome. Plant J. *72*, 523–536.

Oparka, K.J., Duckett, C.M., Prior, D.A.M., and Fisher, D.B. (1994). Real-time imaging of phloem unloading in the root tip of *Arabidopsis*. Plant J *6*, 759–766.

Overvoorde, P., Fukaki, H., and Beeckman, T. (2010). Auxin control of root development. Cold Spring Harb. Perspect. Biol. *2*, a001537.

Perilli, S., and Sabatini, S. (2010). Analysis of root meristem size development. Methods Mol. Biol. *655*, 177–187.

Pickett, F.B., Wilson, A.K., and Estelle, M. (1990). The *aux1* mutation of *Arabidopsis* confers both auxin and ethylene resistance. Plant Physiol. *94*, 1462–1466.

Robert, H.S., Grones, P., Stepanova, A.N., Robles, L.M., Lokerse, A.S., Alonso, J.M., Weijers, D., and Friml, J. (2013). Local auxin sources orient the apical-basal axis in *Arabidopsis* embryos. Curr. Biol. *23*, 2506–2512.

Roman, G., Lubarsky, B., Kieber, J.J., Rothenberg, M., and Ecker, J.R. (1995). Genetic analysis of ethylene signal transduction in *Arabidopsis thaliana*: five novel mutant loci integrated into a stress response pathway. Genetics *139*, 1393–1409.

Růzicka, K., Ljung, K., Vanneste, S., Podhorská, R., Beeckman, T., Friml, J., and Benková, E. (2007). Ethylene regulates root growth through effects on auxin biosynthesis and transport-dependent auxin distribution. Plant Cell *19*, 2197–2212.

Sarkar, A.K., Luijten, M., Miyashima, S., Lenhard, M., Hashimoto, T., Nakajima, K., Scheres, B., Heidstra, R., and Laux, T. (2007). Conserved factors regulate signalling in *Arabidopsis thaliana* shoot and root stem cell organizers. Nature *446*, 811–814.

Stepanova, A.N., Hoyt, J.M., Hamilton, A.A., and Alonso, J.M. (2005). A link between ethylene and auxin uncovered by the characterization of two root-specific ethylene-insensitive mutants in *Arabidopsis*. Plant Cell *17*, 2230–2242.

Stepanova, A.N., Robertson-Hoyt, J., Yun, J., Benavente, L.M., Xie, D.Y., Dolezal, K., Schlereth, A., Jürgens, G., and Alonso, J.M. (2008). TAA1-mediated auxin biosynthesis is essential for hormone crosstalk and plant development. Cell *133*, 177–191.

Stepanova, A.N., Yun, J., Likhacheva, A.V., and Alonso, J.M. (2007). Multilevel interactions between ethylene and auxin in *Arabidopsis* roots. Plant Cell *19*, 2169–2185.

Stepanova, A.N., Yun, J., Robles, L.M., Novak, O., He, W., Guo, H., Ljung, K., and Alonso, J.M. (2011). The *Arabidopsis* YUCCA1 flavin monooxygenase functions in the indole-3-pyruvic acid branch of auxin biosynthesis. Plant Cell *23*, 3961–3973.

Swarup, R., Perry, P., Hagenbeek, D., Van Der Straeten, D., Beemster, G.T., Sandberg, G., Bhalerao, R.P., Ljung, K., and Bennett, M.J. (2007). Ethylene upregulates auxin biosynthesis in *Arabidopsis* seedlings to enhance inhibition of root cell elongation. Plant Cell *19*, 2186–2196.

Swarup, K., Benková, E., Swarup, R., Casimiro, I., Péret, B., Yang, Y., Parry, G., Nielsen, E., De Smet, I., Vanneste, S., et al. (2008). The auxin influx carrier LAX3 promotes lateral root emergence. Nat. Cell Biol. *10*, 946–954.

Tao, Y., Ferrer, J., Ljung, K., Pojer, F., Hong, F., Long, J.A., Li, L., Moreno, J.E., Bowman, M.E., Ivans, L.J., et al. (2008). Rapid synthesis of auxin via a new tryptophan-dependent pathway is required for shade avoidance in plants. Cell *133*, 164–176.

Teale, W.D., Paponov, I.A., and Palme, K. (2006). Auxin in action: signalling, transport and the control of plant growth and development. Nat. Rev. Mol. Cell Biol. *7*, 847–859.

Turnbull, C.G.N., Booker, J.P., and Leyser, H.M.O. (2002). Micrografting techniques for testing long-distance signalling in *Arabidopsis*. Plant J. *32*, 255–262.

Ulmasov, T., Murfett, J., Hagen, G., and Guilfoyle, T.J. (1997). Aux/IAA proteins repress expression of reporter genes containing natural and highly active synthetic auxin response elements. Plant Cell *9*, 1963–1971.

Vaseva, I.I., Qudeimat, E., Potuschak, T., Du, Y., Genschik, P., Vandenbussche, F., and Van Der Straeten, D. (2018). The plant hormone ethylene restricts Arabidopsis growth via the epidermis. Proc. Natl. Acad. Sci. USA, p.201717649.

Villarino, G.H., Hu, Q., Manrique, S., Flores-Vergara, M., Sehra, B., Robles, L., Brumos, J., Stepanova, A.N., Colombo, L., Sundberg, E., et al. (2016). Transcriptomic signature of the *SHATTERPROOF2* expression domain reveals the meristematic nature of *Arabidopsis* gynoecial medial domain. Plant Physiol. *171*, 42–61.

Waese, J., and Provart, N.J. (2016). The Bio-Analytic Resource: data visualization and analytic tools for multiple levels of plant biology. Curr. Plant Biol. *7–8*, 2–5.

Weijers, D., Sauer, M., Meurette, O., Friml, J., Ljung, K., Sandberg, G., Hooykaas, P., and Offringa, R. (2005). Maintenance of embryonic auxin distribution for apical-basal patterning by PIN-FORMED-dependent auxin transport in *Arabidopsis*. Plant Cell *17*, 2517–2526.

Yamada, M., Greenham, K., Prigge, M.J., Jensen, P.J., and Estelle, M. (2009). The *TRANSPORT INHIBITOR RESPONSE2* gene is required for auxin synthesis and diverse aspects of plant development. Plant Physiol. *151*, 168–179.

Zhao, Y., Christensen, S.K., Fankhauser, C., Cashman, J.R., Cohen, J.D., Weigel, D., and Chory, J. (2001). A role for flavin monooxygenase-like enzymes in auxin biosynthesis. Science *291*, 306–309.

Zhao, Y. (2014). Auxin biosynthesis. In The *Arabidopsis* Book (American Society of Plant Biologists), p. e0173.

Zhou, Z.Y., Zhang, C.G., Wu, L., Zhang, C.G., Chai, J., Wang, M., Jha, A., Jia, P.F., Cui, S.J., Yang, M., et al. (2011). Functional characterization of the *CKRC1/TAA1* gene and dissection of hormonal actions in the *Arabidopsis* root. Plant J. *66*, 516–527.

STAR★METHODS

KEY RESOURCES TABLE

REAGENT	SOURCE	IDENTIFIER
Bacterial and Virus Strains		
One Shot TOP10 Chemically Competent cells, *Escherichia coli*	Life Technologies	C404010
Agrobacterium tumefaciens (strain C-58)	Lab stock	N/A
Chemicals, Peptides, and Recombinant Proteins		
Triton X-100	Sigma – Aldrich	X100-500ML
Bleach (Sodium hypochlorite 6%)	Pure Bright 6%	Germicidal Ultra Bleach
Agarose Low Melting	Thermo - Fisher	BP1360-100
Murashige and Skoog basal salts	Caisson Labs	MSP01
Sucrose	Thermo - Fisher	S5-12
Agar granulated	Difco	214510
1-Aminocyclopropanecarboxylic acid (ACC)	PhytoTechnology Labs	A1180
3-Indoleacetic acid	Sigma – Aldrich	I3750
Naphthalene-1-acetic acid (NAA)	Sigma – Aldrich	N0640
N-1-Naphthylphthalamidic acid (NAA)	Sigma – Aldrich	PS343
1-Naphthoxyacetic acid (1-NOA)	Sigma – Aldrich	255416
L-Kynurenine (Kyn)	Sigma – Aldrich	K8625
Yucasin	Dr. Koshiba	Nishimura et al. (2014)
Propidium iodide	Sigma – Aldrich	P-4170
Acetone	Thermo - Fisher	A11-4
Safranin-0	Thermo - Fisher	S670
Glycerol	Thermo - Fisher	BP229
Potassium ferricyanide	MP BIOMEDICALS	2152559
Potassium ferrocyanide trihydrate	MP BIOMEDICALS	2152560
X-Gluc	Gold Biotechnology	G1281C4
Urea	Sigma – Aldrich	U-6504
Xylitol	Acros	225981000
Deoxycholic acid sodium salt	G-Biosciences	DG090
Carboxyfluorescein diacetate (CFDA)	Thermo - Fisher	50520723
Ethyl alcohol	Pharmco Aaper	111ACS200
Lanolin	Now Solutions	7725
Critical Commercial Assays		
pENTR/D-TOPO Cloning Kit	Life Technologies	K240020
Gateway LR Clonase II enzyme mix	Life Technologies	11791019
iProof High-Fidelity DNA Polymerase 100U	Bio-Rad	1725301
Experimental Models: Organisms/Strains		
Arabidopsis thaliana: WT Col-0	Lab stock	CS70000
Arabidopsis thaliana: mutants	Table S1	N/A
Oligonucleotides		
Primers for genotyping	Table S1	N/A
Primers for cloning	Table S2	N/A
Recombinant DNA		
pGWB2	Nakagawa et al. (2007)	N/A
pGWB4	Nakagawa et al. (2007)	N/A

(*Continued on next page*)

Continued

REAGENT	SOURCE	IDENTIFIER
Software and Algorithms		
ImageJ	ImageJ	https://imagej.net/Fiji/Downloads
Zen	Zeiss	https://www.zeiss.com
Statistical Calculators	Astatsa	http://astatsa.com
Q Capture Software	Q Imaging	https://www.qimaging.com

CONTACT FOR REAGENT AND RESOURCE SHARING

Further information and requests for resources and reagents should be directed to and will be fulfilled by the Lead Contact, Anna N. Stepanova (atstepan@ncsu.edu).

EXPERIMENTAL MODEL AND SUBJECT DETAILS

Strains and Genotyping

A majority of Arabidopsis genotypes employed in this work are in Columbia ecotype Col-0, including controls (WT), mutant strains and transgenic lines, unless indicated otherwise. Mutant lines *wei8-1, wei8-2, tir2-1, tar2-1, wei8-1 tar2-1, wei8-2 tar2-1, and wei8-1 tar2-1 DR5:GFP* were previously reported (Stepanova et al., 2008; Yamada et al., 2009); *pin* single mutants and *lax1* were obtained from ABRC (Alonso et al., 2003), *aux1*-7 mutant (Pickett et al., 1990) came from the Ecker lab stock (see Table S1). Double mutants were generated by crossing *wei8-1* to the single transporter mutants and identified by genotyping and/or phenotyping in F2 and F3. The *WEI8p$_{(3.4)}$:WEI8$_{cDNA}$-GUS* line was provided by Dr. Estelle (Yamada et al., 2009). Infertile *wei8 tar2* mutants and transgenic lines were maintained as *wei8 tar2*/+ sesquimutants, selected phenotypically in three-day-old dark-grown plants, and the homozygosity of the *tar2* mutation was confirmed genotypically, Genotyping of DNA samples extracted from various T-DNA mutants, transgenic lines and their derivatives was performed by PCR. The origin of all mutant alleles used in this study and their respective genotyping primers are listed in Table S1.

To genotype mutant lines, genomic DNAs were extracted using the cetyltrimethylammonium bromide (CTAB) method in 96-well plates. Plant tissues were collected into the individual wells, frozen at -80°C, ground in a Qiagen shaker with 4.5 mm steel zinc beads, and resuspended in 250 μL of CTAB buffer (1.4 M NaCl, 20 mM EDTA, 100 mM Tris-HCl, pH 8, 3% CTAB, Calbiochem). Samples were incubated at 65°C for 30 min, extracted once with 1 volume of chloroform, and precipitated with 1 volume of isopropyl alcohol. DNA containing pellets were washed once with 70% ethanol, air-dried, and resuspended in 200 μL of deionized water.

A standard 10μL PCR reaction included 1 μL of 10x PCR buffer, 0.25 μL of 2 mM dNTPs, 0.25 μL of Taq polymerase, 0.25 μL of 20 μM forward primer, 0.25 μL of 20 μM reverse primer, 1 μL of genomic DNA, and 7 μL of H2O. A common PCR program was (30 s at 94C, 30 s at 56C, 1 to 3 min at 72C [1 min per kb]) times 40 cycles. PCR products were resolved on 1x Tris-acetate-EDTA 1% agarose gels.

METHOD DETAILS

Recombineering Translational Fusion Lines

Bacterial recombineering (Alonso and Stepanova, 2015) as employed to introduce *YPet* or *GUS* reporters into transformable BAC clones and to trim 5' and 3' ends of the constructs. To generate the gDNA and cDNA constructs of *WEI8* with *YPet*, we first trimmed a *WEI8*-containting JAtY clone JAtY73L21 using the primers At1g70560DelLeft and replaRB_amp_ universal to remove extra sequences adjacent to the Right Border site and the primers At1g70560DelRight and replaLB_tet_universal to remove the sequences adjacent to the Left Border side of this JAtY clone, producing a trimmed untagged *WEI8$_{gDNA}$* clone with 10Kb upstream of the start codon and 5kb downstream of the stop codon of *WEI8*. The deletions were confirmed using the primers At1g70560TestDelRight and LBtest and At1g70560TestDelLeft and RBtest. Next, to generate an equivalent *WEI8$_{cDNA}$* clone, the genomic sequences corresponding to the coding region of *WEI8* with all of its introns in *WEI8$_{gDNA}$* were replaced by a selectable/contra-selectable cassette amplified with the primers TAA1intlessF and TAA1intlessR. This cassette was then replaced by the *WEI8* cDNA sequences amplified from a cDNA pENTR/D-Topo clone (Stepanova et al., 2008) using the primers TAA1startcDNA and TAA1endcDNA. Finally, the *YPet* cassette was introduced at the N-terminus of both *WEI8$_{gDNA}$* and *WEI8$_{cDNA}$* clones using the primers At1g70560F and At1g70560R, producing *WEI8p:YPet-WEI8$_{gDNA}$* and *WEI8p:YPet-WEI8$_{cDNA}$*. The insertion was confirmed by PCR using the primers At1g70560TestF and At1g70560TestR and subsequent re-sequencing of the entire cDNA and *YPet* sequences and the corresponding junctions.

To make a *YUC3* construct with *GUS*, *YUC3p:YUC3$_{gDNA}$-GUS*, we trimmed the RB side of the TAC clone JAtY72A20 using the primers At1g04610TestDelLeft and replaRB_amp_universal. This deletion was confirmed using the primers At1g04610TestDelLeft and RBtest. The *GUS* cassette was then inserted immediately upstream of the stop codon of this gene using the primers At1g04610F and At1g04610R to make a C-terminal fusion with *GUS*. The insertion was confirmed by PCR using the primers

At1g04610TestF and At1g04610TestR and by resequencing of the *GUS* coding region and junction sequences. The same general strategy was used to tag the *WEI8* and *TAR2* genes with the *GUS* cassette in the context of TAC clones JAtY73L21 and JAtY76L22, respectively, except that in these cases the reporter was inserted immediately downstream of the translation start codon to make N-terminal translational fusions with *GUS*. The primers employed for the trimming of the *WEI8* TAC, for the insertion of *GUS* in the N-terminus, and for testing of the final product were the same as the ones used for generating the *YPet* construct, *WEI8p:YPet-WEI8*$_{gDNA}$, producing *WEI8p:GUS-WEI8*$_{gDNA}$. To make the *TAR2* fusion with *GUS*, *TAR2p:GUS-TAR2* $_{gDNA}$, the primers utilized followed the same nomenclature as those used for *YUC3*, replacing the At1g04610 ID number of *YUC3* with the At4g24670 ID number of *TAR2*. The corresponding primer sequences used for trimming and tagging of all aforementioned recombineering constructs are shown in Table S2.

wei8-2 tar2-1/+ was transformed with *WEI8p:YPet-WEI8*$_{gDNA}$ and *WEI8p:YPet-WEI8*$_{cDNA}$, and Col-0 was transformed with *WEI8p:GUS-WEI8*$_{gDNA}$, *TAR2p:GUS-TAR2* and *YUC3p:YUC3-GUS* using a modified *Agrobacterium*-mediated "flower-dip" method (Alonso and Stepanova, 2014). Homozygotes were identified in T3 based on Basta resistance, YPet fluorescence or GUS staining and confirmed by genotyping. Assays were performed in T3 and T4 plants. Two or more independent lines were characterized for each construct.

Plant Growth Conditions and Physiological Assays

For seedling assays, seeds were surface-sterilized for 15 minutes using 50% bleach spiked with 0.01% Triton X-100 to avoid seed clumping, washed six times with sterile deionized water, resuspended in melted pre-cooled 0.7% low-melting-point agarose in water and planted on the surface of AT control plates (4.33 g/L Murashige and Skoog salts, 10 g/L sucrose, pH raised to 6.0 with 1 M KOH, and 7 g/L Bacto Agar) supplemented with the following additives: 10 μM ACC [Phytotechnology Lab], 100 nM IAA, 50 nM NAA, 10 μM NPA, 30 μM 1-NOA, 1 to 25 μM L-Kynurenine [Sigma-Aldrich] and/or 25 μM yucasin (gift from Dr. Koshiba (Nishimura et al., 2014)), as indicated in figure legends. Plates with seeds were kept at 4°C for 3 d, light-treated (120 μmol/m^2/sec) for 1 h at 20°C to equalize germination, stacked and placed horizontally in the dark at 22°C. After 72 h of growth in the dark, phenotypes were analyzed, plants photographed, and representative samples collected for 3-day-old dark-grown seedlings. Late-germinating seedlings were removed and discarded, and plates with the remaining seedlings were placed vertically under constant light (120 μmol/m^2/sec) at 20°C. After an additional 7-day-period, pictures were taken, phenotypes scored, and samples collected for 10-day-old light-grown seedlings. To assess root meristem viability after the 10-day NPA treatment, seedlings were transferred to either control or NPA-supplemented vertical plates for 4 more days and at 14 days of age evaluated by confocal microscopy. To evaluate adult phenotypes and for seed propagation, plate-germinated seedlings were transferred to soil (a 50:50 mix of Fafard 4P (Fafard) and Sunshine Professional Growing Mix (Sun Gro Horticulture)) and grown under a 16 h light/8 h dark cycle (120 μmol/m^2/sec) at 20°C.

Microscopy

To analyze primary root meristem phenotypes and to monitor GFP/YPet fluorescence and Propidium Iodide (PI) signals, Zeiss Zen software running a Zeiss LSM 710 confocal microscope with a 40x water objective (1.1 N.A.) was used. The excitation/emission wavelengths during acquisition were 488 nm/493–536 nm for GFP/YPet and 561 nm/615–716 nm for PI. For picture acquisition, seedlings were incubated in 10 mg/ml PI in water for 5 minutes and mounted in distilled water. For routine fluorescence analysis, transgenic seedlings were monitored using a Zeiss Axioplan epifluorescence microscope. Root, stamen, and pistil length quantifications were done using NIH ImageJ software (National Institutes of Health, USA. http://imagej.nih.gov/ij) on photographs taken with Q Capture software on a 5.0 RTV digital camera (Q Imaging, Surrey, BC, Canada) mounted on a slide under a dissecting scope. The same equipment and software were used to quantify cotyledon and leaf vasculature. Detached organs were fixed in ice-cold 90% acetone for 1 hour and washed in 95% ethanol for 1 hour. Cotyledons were stained using 1% Safranin-0 in ethanol, samples were destained in ethanol series (95-70-30-10%) in water for 2 minutes each and mounted in 50% glycerol. Leaves were optically cleared with ClearSee solution (Kurihara et al., 2015).

To evaluate root phenotypes and to quantify meristem cell numbers (Perilli and Sabatini, 2010), an Axioscop2 microscope (Zeiss) with Nomarski optics was used. Seedlings were fixed in 4% paraformaldehyde and cleared using ClearSee solution (Kurihara et al., 2015). For GUS staining, seedlings were fixed in ice-cold 90% acetone, washed once with rinse solution (50 mM NaPO4 buffer, pH 7.0, 0.5 mM K3Fe(CN)6, and 0.5 mM K4Fe(CN)6), then vacuum-infiltrated with the staining solution (rinse solution supplemented with 1 mg/mL 5-Bromo-4-chloro-3-indolyl β-D-glucuronide cyclohexylammonium salt) and left staining from 4 to 14 hours until staining became noticeable. To stop the staining reaction, ethanol was added to a 15% final concentration. Seedlings were tapped dry on a paper towel and optically cleared using ClearSee solution for 7 days. Representative seedlings were photographed.

CryoSEM Imagining

CryoSEM images were taken using a JEOL JSM-7600 FE SEM (JEOL USA, Peabody, MA) outfitted with Alto-2500 (Gatan, Warrendale, PA). Samples were dissected and attached to the holder using Optimal Cutting Temperature compound (OCT) [Fisher-Scientific]. The samples were plunge frozen in liquid nitrogen slush, transferred under vacuum to the Alto-2500 preparation chamber, etched for 10 min at -96°C under 4 x 10^{-6} mbar vacuum to reveal microstructures, and cooled down to -120°C. An in-situ cold magnetron coater was used to make a 5 nm thickness Au/Pd coating on etched samples. The SEM images were taken using 5 kV energy at 30 mm working distance under cryo-temperature.

Grafting

Grafts of WT *DR5*:*GFP* and *wei8-1 tar2-1 DR5:GFP* scions and rootstocks were performed using the transverse cut-and-butt alignment method (Turnbull et al., 2002) with minor modifications. WT *DR5*:*GFP* and *wei8-1 tar2-1*/+ *DR5:GFP* seeds were germinated in the dark for 3 days at 22°C on control low-sucrose plates (0.5% sucrose) supplemented with 10 μM 1-aminocyclopropane-1-carboxylic acid (ACC) to rapidly score *wei8-1 tar2-1*. Seedlings were then moved to light for 16 hours to allow the cotyledons to open before grafting and transferred to Petri dishes containing sterile water-saturated No. 1 Whatman filter paper discs to keep seedlings moist and provide a solid surface to perform the cuts. The procedure was conducted in a laminar flow hood to keep sterile conditions. One cotyledon was removed from every scion to facilitate alignment of the graft and minimize subsequent scion-rootstock separation due to cotyledon growth. A transverse cut was made on the middle of the hypocotyl using a Swann medical surgical blade No. 15. Grafts were carefully aligned and assembled with no supporting collar on control low-sucrose medium with the aid of a dissecting scope. Plates were sealed with Parafilm and kept vertically at 26°C under short-day conditions (8 hr of 80 μmol/m^2/sec light) for at least 10 days. Graft connections were assessed by gently pulling on the scions and if the rootstocks remained attached, the grafting was considered successful. *DR5:GFP* fluorescence was monitored using a Zeiss Axiophot epifluorescence microscope. After primary root phenotypes were scored and photographed, Xylem connectivity was examined by the CFDA assay (Oparka et al., 1994). After 30 minutes of feeding roots with 1 mM CFDA, fluorescence in the cotyledon vasculature was monitored. Graft connections, *DR5:GFP* fluorescence, and root phenotypes were analyzed again 21 days after grafting. Detached roots of WT *DR5*:*GFP* and *wei8-1 tar2-1 DR5:GFP* seedlings were used as negative controls. The efficiency of grafting varied between different combinations, with grafting deemed successful if the vasculature reconnected. Connection was determined by pulling on the scions. The best combinations were WT:WT and *wei8 tar2*:WT grafts with a grafting success rate of 55%, whereas *wei8 tar2:wei8 tar2* had a success rate of 42%. In the latter combination, the root meristems always degenerated. In contrast, the success rate of the WT:*wei8 tar2* graft was only 9%, the lowest of all combinations analyzed (scion and rootstock vasculature did re-attach, but the root meristem always degenerated). The growth of WT adventitious roots was likely in part responsible for the rejection of the grafted mutant roots in the WT:*wei8 tar2* combination. On average, around 15-25 seedlings were grafted per experiment for each of the combinations with the higher success rate. For the most challenging combination, WT:*wei8 tar2*, more than 60 seedlings were grafted per experiment. In total, four different grafting experiments were performed and evaluated, with a combined number of 20 or more successfully grafted plants examined for each genotype combination across the four replicates. A subset of *wei8 tar2*/WT grafted seedlings was transferred to soil to monitor rosette growth of grafted plants.

A Cre/Lox-Based System to Induce Local Auxin Biosynthesis

The original transgenic *Cre/Lox≫iaaM/GUS* line provided by Dr. Eva Benkova (Dubrovsky et al., 2008) is in a mixed Col/Ler background and harbors the following four components: (1) CRE recombinase under the control of the Arabidopsis heat shock-inducible promoter *HSP18.2* (Heidstra et al., 2004); (2) a *GAL4*::*VP16* synthetic transcriptional activator separated from the constitutive *35S* promoter by a spacer flanked with *loxP* sites (Heidstra et al., 2004); (3) a *UAS*-promoter driven *GUS* reporter; and (4) a *UAS*-promoter driven bacterial auxin biosynthesis gene *iaaM* (Weijers et al., 2005). Herein, a 5th element, the bacterial auxin biosynthesis gene *iaaH* under a control of a *UAS* promoter, was introduced via *Agrobacterium*-mediated transformation to complete the bacterial auxin biosynthesis pathway and enhance the production of auxin in transgenic plants upon heat shock. Thus, the new *Cre/Lox≫iaaM/iaaH/GUS* line harbors the entire bacterial auxin biosynthesis pathway inducible by heat stress. The induction of auxin production was monitored by GUS staining and plant phenotyping. To generate *UASp:iaaH*, the *iaaH* gene was amplified from a template provided by the Scheres group by PCR (see Table S2 for primer sequences) and subcloned in a pENTR/D-Topo (Invitrogen), confirmed by sequencing, and recombined into pUAS-pGWB2 (Villarino et al., 2016) using LR Clonase II (Invitrogen).

Heat shock was applied to shoots or roots to locally upregulate the expression of *iaaM*/*iaaH* bacterial auxin biosynthetic genes. Treatments were performed on plates containing 3-day-old dark-grown seedlings. Plates were placed in two different water-bath/air conditions to selectively induce the system either in roots or in shoots, or left untreated as a no-induction control. For these experiments, a small water bath set to 20°C was kept inside of the oven adjusted to 60°C. The plates were floating on the surface of the water bath and the measured temperature in the plate media was 20°C after a few minutes in the bath. This temperature prevented the induction of the system in the roots. The temperature at the interface between the media and the air (calculated from a gradient between the air and media temperature), estimated to be around 37-40°C, was sufficient to trigger the system induction. The optimal temperatures utilized in this assay were empirically determined and air temperatures below 50°C did not result in shoot activation of the Cre-Lox system. For the activation of the system in roots, the plates were floating in a water bath at 37°C and the temperature of the media in this case was also around 37°C, while the air temperature was set to 4°C to avoid induction in the shoot. The duration of the treatments was 90 minutes. To test the effect of the different heat shock treatments, control seedlings were kept at 24°C. To assess the role of local auxin production triggered by the inducible system, seedlings were germinated on 25 μM L-kynurenine and 25 μM yucasin, gift from Dr. Koshiba (Nishimura et al., 2014) to inhibit endogenous auxin biosynthesis or on Control plates. In parallel, some WT seedlings germinated on kynurenine-yucasin or on Control plates were heat-shocked to determine the effect of heat-shock treatments on root morphology in the absence of *Cre/Lox≫iaaM/iaaH/GUS transgenes*. Primary root meristem phenotypes and GUS staining patterns were analyzed in 10-day-old seedlings, i.e. 7 days after the heat-shock treatments.

Auxin Applications to Apical Shoot

Liquid lanolin (Now Solutions) at 40 °C was mixed with 10mM auxin to obtain a final concentration of 2 mM IAA. A 1 μl drop of the supplemented lanolin solidified during application on the apical shoot of 3-day-old Col-0 wild type and *wei8-1 tar2-1* double mutant seedlings. A second drop was applied at 6 days post germination. Control treatments were performed with lanolin supplemented with the auxin solvent ethanol. Primary, lateral and adventitious root meristem phenotypes were analyzed in 14- and 21-day-old seedlings.

Tissue-Specific *WEI8* Expression Lines Using *WOX5*, *UBQ10*, and *WER* Promoters

The promoter of *WUSCHEL RELATED HOMEOBOX5 (WOX5p)*, a well-characterized quiescent center marker (Blilou et al., 2005; Sarkar et al., 2007), was used to confine the expression of *WEI8* to this group of cells. *WOX5p* (4660bp) was PCR-amplified by iProof (Bio-Rad) from genomic DNA using primers WOX5P_S1 and WOX5pRev (primers are shown in Table S2) and the PCR product was subcloned in a pENTR/D-Topo (Invitrogen) vector following manufacturer's protocols. The *pENTR-WOX5p* construct was confirmed by sequencing using M13For, M13Rev, and internal primers: WOX5pt1R, WOX5pt2F, WOX5pt2R, WOX5pt3F, WOX5pt3R (See Table S2 for primer sequences). A PCR-based approach was employed to join the last 1561bp of the *WOX5p* 3' end with the 1173bp *WEI8* cDNA already subcloned in a pENTR/D-Topo vector (Stepanova et al., 2008). To generate the fused DNA fragment, three PCR reactions were performed: PCR 1 with primers WOX5-pt3F and WOX5Reverse with *WEI8* tail; PCR 2 with primers TAA1Forward with WOX5 tail and M13Rev; and the fusion PCR 3 to join together both fragments using the external primers WOX5-Pt3F and M13Reverse (Primer information is present in Table S2). The product of the fusion PCR was double-digested with *NcoI*/*AscI* and ligated into the *NcoI*/*AscI*-open pENTR-WOX5p vector to generate the *WOX5p:WEI8* fusion in pENTR/D-Topo vector. LR Clonase II (Invitrogen) reaction was performed to move the *WOX5p:WEI8* cDNA fragment into pGWB4 (Nakagawa et al., 2007) generating the construct *WOX5p:WEI8-GFP*. Homozygous single-insertion transgenic lines harboring this construct were obtained in T3 generation in the *wei8-1 tar2-1*/+ sesquimutant background. Three independent lines were characterized.

Transgenic lines in the *wei8-1* background with *WEI8* expression under the control of *WEREWOLF* promoter *(WERp)* to limit *WEI8 expression* to the epidermis or under the *UBIQUITIN10* promoter *(UBQ10p)* to drive constitutive expression of *WEI8* throughout the entire root were provided by Dr. Jose Dinneny (Bao et al., 2014). Both lines have been shown to complement the hydropatterning defect phenotypes of *wei8-1* (Bao et al., 2014). These original lines were crossed to *wei8-1 tar2-1*/+ *DR5:GFP* to obtain *wei8-1 tar2-1*/+ *WERp:WEI8* DR5:GFP and *wei8-1 tar2-1*/+ *UBQ10p:WEI8 DR5:GFP*. *WOX5p:GFP* and *WERp:GFP* in Col background were used as controls and were provided by Drs. Ross Sozzani (de Luis Balaguer et al., 2017) and Terri Long (Dinneny et al., 2008), respectively.

QUANTIFICATION AND STATISTICAL ANALYSIS

All datasets are averages of four or more biological replicates (two to three separate experiments performed on two to four independent seed batches per genotype per experiment). Statistical parameters, such as n, the minimal number of plants analyzed for all replicates combined, are indicated in the figure legends. In all graphs, bars represent means (unless otherwise stated) ± SD. Statistical analysis was performed in Excel. Data were analyzed by ANOVA Pairwise post-hoc Tukey HSD (Montgomery, 2012) for comparing multiple treatments. Asterisks in graphs indicate the level of significance of p-value < 0.05, unless otherwise stated.